NANO MICRO
small

Supporting Information

for *Small,* DOI: 10.1002/smll.201907688

Nuclear Mechanics within Intact Cells Is Regulated by Cytoskeletal Network and Internal Nanostructures

Jitao Zhang, Farid Alisafaei, Miloš Nikoli#, Xuefei A. Nou, Hanyoup Kim, Vivek B. Shenoy, and Giuliano Scarcelli**

Supporting Information

Nuclear mechanics within intact cells is regulated by cytoskeletal network and internal nanostructures

Jitao Zhang,[1†] Farid Alisafaei,[2,3†] Miloš Nikolić,[4] Xuefei A. Nou,[1] Hanyoup Kim,[5] Vivek B. Shenoy[2,3] and Giuliano Scarcelli [1,4*]*

[1] Fischell Department of Bioengineering, University of Maryland, College Park, MD 20742, USA.

[2] Department of Materials Science and Engineering, School of Engineering and Applied Science, University of Pennsylvania, PA, 19104, USA.

[3] Center for Engineering Mechanobiology, University of Pennsylvania, PA, 19104, USA.

[4] Maryland Biophysics Program, University of Maryland, College Park, MD 20742, USA.

[5] Canon U.S. Life Sciences, Inc., 9800 Medical Center Drive, Suite C-120, Rockville, MD 20850, USA.

[†] These authors contributed equally to this work.

[*] V.B.S. vshenoy@seas.upenn.edu; G. S. scarc@umd.edu.

Supplementary Note 1: Three-Dimensional Chemomechanical Model

To study how disruption of cytoskeletal components impacts nuclear mechanics, we develop a coarse-grained chemomechanical model that accounts for the key cellular components involved in the transmission of physical signals from the ECM to the nucleus including (i) the cytoskeleton, (ii) the nucleus, and (iii) the focal adhesions (see Fig. 3). In the following sections, we present the constitutive equations of these components. The model will be implemented in a finite element framework.

1. Cytoskeleton

The cytoskeleton in our model is composed of three elements including (i) the myosin motors, (ii) the microtubules, and (iii) the actin filaments (see Fig. 3).

1.1 Myosin motors

The contractile force generated by an individual phosphorylated myosin motor can be modeled as a force dipole which is a pair of equal but oppositely directed forces (see Fig. 3A). The spatial density of these force dipoles in our coarse-grained model is treated as a symmetric tensor ρ_{ij} whose components represent cell contractility in different directions [1,2]. As shown in equation (1) in the main text, the average of contractility in all three directions, $\frac{1}{3}\rho_{kk} = (\rho_{11} + \rho_{22} + \rho_{33})/3$, is related to the average of stress in the actin filaments network, $\frac{1}{3}\sigma_{kk} = (\sigma_{11} + \sigma_{22} + \sigma_{33})/3$, and the anisotropy in the components of the stress tensor, σ_{a}, as follows

$$\frac{\rho_{kk}}{3} = f_{\mathrm{m}}\frac{\sigma_{kk}}{3} + f_{\mathrm{a}}\sigma_{\mathrm{a}} + f_0\,\rho_0 \tag{S1.1}$$

where this stress-dependent feedback mechanism is regulated by the feedback parameters f_{m} and f_{a}, while in the absence of tension ($\sigma_{kk} = 0$), f_0 regulates the mean contractility $\frac{1}{3}\rho_{kk}$ and relates it to the cell contractility in the quiescent state (initial contractility) ρ_0. Here, we explicitly define the contractility tensor ρ_{ij} and the stress tensor σ_{ij} as functions of strain tensors $\varepsilon_{ij}^{(\mathrm{X})}$ and $\varepsilon_{ij}^{(\mathrm{Y})}$. Note that $\varepsilon_{ij}^{(\mathrm{X})}$ and $\varepsilon_{ij}^{(\mathrm{Y})}$ are the strain tensors of cytoskeletal components that are in compression

(e.g., microtubules) and tension (e.g., actin filaments), respectively. Fig.S9 shows $\varepsilon^{(X)}$ and $\varepsilon^{(Y)}$ which are one-dimensional representations of strain tensors $\varepsilon_{ij}^{(X)}$ and $\varepsilon_{ij}^{(Y)}$.

To capture the fact that cell contractility increases with tension, the cell contractility tensor ρ_{ij} is defined in our model as a function of the strain tensor $\varepsilon_{ij}^{(X)}$ as follows

$$\rho_{ij} = K^{(\rho)}\varepsilon_{kk}^{(X)}\delta_{ij} + 2\mu^{(\rho)}\left(\varepsilon_{ij}^{(X)} - \frac{1}{3}\varepsilon_{kk}^{(X)}\delta_{ij}\right) + \bar{\rho}_0\delta_{ij} \tag{S1.2}$$

where $K^{(\rho)}$, $\mu^{(\rho)}$, and $\bar{\rho}_0$ are the motor density effective modulus, the polarization effective modulus, and the effective contractility

$$K^{(\rho)} = \frac{3K^{(MT)}\alpha_v - 1}{3(\beta_v - \alpha_v)} \quad , \quad \mu^{(\rho)} = \frac{2\mu^{(MT)}\alpha_d - 1}{2(\beta_d - \alpha_d)} \quad , \quad \bar{\rho}_0 = \frac{\beta_v\,\rho_0}{\beta_v - \alpha_v} \tag{S1.3}$$

which are related to $K^{(MT)}$ (the bulk modulus of the cytoskeletal components that are in compression), $\mu^{(MT)}$ (the shear modulus of the cytoskeletal components that are in compression), α_v (the volumetric chemo-mechanical feedback parameter), α_d (the deviatoric chemo-mechanical feedback parameter), β_v (the volumetric chemical stiffness), and β_d (the deviatoric chemical stiffness) [1,2].

1.2. Microtubules

Consistent with experimental observations where microtubules are compressively loaded by the internally generated cell contractile forces [3], in our coarse-grained model, the cell contractility ρ_{ij} applies the compressive stress $C_{ijkl}^{(MT)}\varepsilon_{kl}^{(X)}$ on the microtubule network where $\mathbf{C}^{(MT)}$ is the stiffness tensor of the microtubule network

$$C_{ijkl}^{(MT)} = K^{(MT)}\delta_{ij}\delta_{kl} + \mu^{(MT)}\left(\delta_{ik}\delta_{jk} + \delta_{il}\delta_{jk} - \frac{2}{3}\delta_{ij}\delta_{kl}\right) \tag{S1.4}$$

1.3. Actin filaments

In addition to inducing the compressive stress $C_{ijkl}^{(MT)}\varepsilon_{kl}^{(X)}$ on the microtubule network, the cell contractility ρ_{ij} also generates tensile stress in the actin filament network, σ_{ij} which is transmitted to the extracellular matrix

$$\rho_{ij} = -C_{ijkl}^{(MT)}\varepsilon_{kl}^{(X)} + \sigma_{ij} \tag{S1.5}$$

Note that the cell contractility ρ_{ij} is initially isotropic in our simulations. This indicates that all simulations start with the same contractility in all directions; $\rho_{11} = \rho_{22} = \rho_{33}$. This can be shown by rewriting equation (S1.2) in the following form

$$\rho_{ij} = C_{ijkl}^{(\rho)}\varepsilon_{kl}^{(X)} + \bar{\rho}_0\delta_{ij} \tag{S1.6}$$

where

$$C_{ijkl}^{(\rho)} = K^{(\rho)}\delta_{ij}\delta_{kl} + \mu^{(\rho)}\left(\delta_{ik}\delta_{jk} + \delta_{il}\delta_{jk} - \frac{2}{3}\delta_{ij}\delta_{kl}\right) \tag{S1.7}$$

We can see from equations (S21.5) and (S1.6) that in the stress-free unpolarized state $\sigma_{ij} = 0$, the diagonal components of **ρ** are equal and non-zero $\rho_{11} = \rho_{22} = \rho_{33} \neq 0$, while its off-diagonal components are all zero $\rho_{12} = \rho_{21} = \rho_{13} = \rho_{31} = \rho_{23} = \rho_{32} = 0$. This indicates that the cell contractility ρ_{ij} is initially isotropic and we have the same contractility in all directions in the initial configuration.

As the tensile stress in the actin filament network, σ_{ij}, increases, the stiffness of the actin filament network $C_{ijkl}^{(A)}$ in our model increases to capture the fact that cells actively respond to increasing tension by increasing their own stiffness, which is correlated with recruitment and alignment of actin filaments along the direction of the tensile stress [4,5]. To this end, the stiffness of the actin filament network $C_{ijkl}^{(A)}$ in our model is defined as follows

$$C_{ijkl}^{(A)} = C_{ijkl}^{(I)} + C_{ijkl}^{(F)} \tag{S1.8}$$

where $\mathbf{C}^{(F)}$ represents the tension induced stiffening of the actin network and $\mathbf{C}^{(I)}$ is the initial stiffness of the actin network

$$\mathrm{C}_{ijkl}^{(\mathrm{I})} = K^{(\mathrm{I})}\delta_{ij}\delta_{kl} + \mu^{(\mathrm{I})}\left(\delta_{ik}\delta_{jk} + \delta_{il}\delta_{jk} - \frac{2}{3}\delta_{ij}\delta_{kl}\right) \tag{S1.9}$$

where $K^{(\mathrm{I})}$ and $\mu^{(\mathrm{I})}$ are respectively the initial bulk and shear moduli of the actin network. As $\mathbf{C}^{(\mathrm{F})}$ increases with tension, we first decompose the stress in the actin filament network $\boldsymbol{\sigma}$ as follows

$$\sigma_{ij} = \sigma_{ij}^{(\mathrm{A})} = \sigma_{ij}^{(\mathrm{I})} + \sigma_{ij}^{(\mathrm{F})} \tag{S1.10}$$

where $\boldsymbol{\sigma}^{(\mathrm{I})}$ is linearly related to the strain tensor $\boldsymbol{\varepsilon}^{(\mathrm{Y})}$ using the stiffness tensor $\mathbf{C}^{(\mathrm{I})}$

$$\sigma_{ij}^{(\mathrm{I})} = \mathrm{C}_{ijkl}^{(\mathrm{I})}\,\varepsilon_{kl}^{(\mathrm{Y})} \tag{S1.11}$$

Next, using the following spectral decomposition, we decompose the strain tensor $\boldsymbol{\varepsilon}^{(\mathrm{Y})}$ as follows

$$\boldsymbol{\varepsilon}^{(\mathrm{Y})} = \sum_{i=1}^{3} \varepsilon_i^{(\mathrm{Y})}\,\boldsymbol{n}_i \otimes \boldsymbol{n}_i = \sum_{i=1}^{3} \varepsilon_i^{(\mathrm{Y})}\,\mathbf{E}_i \tag{S1.12}$$

where the orthogonal eigenvectors $\boldsymbol{n}_1$, $\boldsymbol{n}_2$, and $\boldsymbol{n}_3$ are the unit vectors in the directions of the principal strains $\varepsilon_1^{(\mathrm{Y})}$, $\varepsilon_2^{(\mathrm{Y})}$, and $\varepsilon_3^{(\mathrm{Y})}$, respectively. In equation (S1.12), $\otimes$ denotes the dyadic product of two arbitrary vectors $\boldsymbol{u}$ and $\boldsymbol{v}$ as $(\boldsymbol{u} \otimes \boldsymbol{v})_{ij} = u_i v_j$ and the symmetric tensors $\mathbf{E}_1 = \boldsymbol{n}_1 \otimes \boldsymbol{n}_1$, $\mathbf{E}_2 = \boldsymbol{n}_2 \otimes \boldsymbol{n}_2$, and $\mathbf{E}_3 = \boldsymbol{n}_3 \otimes \boldsymbol{n}_3$ are the eigenprojections of the strain tensor $\boldsymbol{\varepsilon}^{(\mathrm{Y})}$. With the eigenvalues $\varepsilon_i^{(\mathrm{Y})}$ and eigenvectors $\boldsymbol{n}_i$ of the strain tensor $\boldsymbol{\varepsilon}^{(\mathrm{Y})}$ at hand, we define the stress tensor $\sigma_{ij}^{(\mathrm{F})}$ in equation (S1.10) as a nonlinear function of the strain tensor $\varepsilon_{ij}^{(\mathrm{Y})}$

$$\boldsymbol{\sigma}^{(\mathrm{F})} = \sum_{i=1}^{3} \frac{\partial f(\varepsilon_i^{(\mathrm{Y})})}{\partial \varepsilon_i^{(\mathrm{Y})}}\,\boldsymbol{n}_i \otimes \boldsymbol{n}_i = \sum_{i=1}^{3} \sigma^{(\mathrm{F})}\left(\varepsilon_i^{(\mathrm{Y})}\right)\mathbf{E}_i = \sum_{i=1}^{3} \sigma_i^{(\mathrm{F})}\mathbf{E}_i \tag{S1.13}$$

where the derivative of the energy function $f(\varepsilon_i^{(\mathrm{Y})})$ is defined in our model as follows

$$\sigma_i^{(\mathrm{F})} = \frac{\partial f(\varepsilon_i^{(\mathrm{Y})})}{\partial \varepsilon_i^{(\mathrm{Y})}} = \tag{S1.14}$$

$$\begin{cases} 0 & \varepsilon_i^{(\mathrm{Y})} < \epsilon_1 \\ \ell\left[\dfrac{\left(\dfrac{\varepsilon_i^{(\mathrm{Y})}-\epsilon_1}{\epsilon_2-\epsilon_1}\right)^t\left(\varepsilon_i^{(\mathrm{Y})}-\epsilon_1\right)^2}{(t+1)(t+2)}\right] & \epsilon_1 \le \varepsilon_i^{(\mathrm{Y})} < \epsilon_2 \\ \ell\left[\dfrac{\left(1+\varepsilon_i^{(\mathrm{Y})}-\epsilon_2\right)^{m+2}-1}{(m+1)(m+2)}+\dfrac{\epsilon_2-\varepsilon_i^{(\mathrm{Y})}}{m+1}+\dfrac{(\varepsilon_i^{(\mathrm{Y})}-\epsilon_2)(\epsilon_2-\epsilon_1)}{t+1}+\dfrac{(\epsilon_2-\epsilon_1)^2}{(t+1)(t+2)}\right] & \varepsilon_i^{(\mathrm{Y})} \ge \epsilon_2 \end{cases}$$

Note that the principal stresses $\sigma_i^{(\mathrm{F})}$ in the above equation vanish for the principal strains $\varepsilon_i^{(\mathrm{Y})}$ below $\epsilon_1 = \epsilon_\mathrm{c} - 0.5\epsilon_\mathrm{t}$ where ϵ_c and $\epsilon_\mathrm{t} = 0.25\epsilon_\mathrm{c}$ are respectively the critical (tensile) principal strain and transition width. For $\epsilon_1 \le \varepsilon_i^{(\mathrm{Y})} < \epsilon_2$, we use a smooth transition function to ensure the continuity and smoothness of $\sigma_i^{(\mathrm{F})} = \partial f/\partial \varepsilon_i^{(\mathrm{Y})}$ at the transition points $\epsilon_1 = \epsilon_\mathrm{c} - 0.5\epsilon_\mathrm{t}$ and $\epsilon_2 = \epsilon_\mathrm{c} + 0.5\epsilon_\mathrm{t}$ where t is the transition constant. For large strains $\varepsilon_i^{(\mathrm{Y})} \ge \epsilon_2$, the principal stress $\sigma_i^{(\mathrm{F})}$ is defined as a nonlinear function of the principal strain $\varepsilon_i^{(\mathrm{Y})}$ with the stiffening parameters ℓ and m.

We now can derive $\mathbf{C}^{(\mathrm{F})}$ using a piecewise linear approximation

$$\mathrm{C}_{ijkl}^{(\mathrm{F})} = \frac{\mathrm{d}\sigma_{ij}^{(\mathrm{F})}}{\mathrm{d}\varepsilon_{kl}^{(\mathrm{Y})}} \qquad \text{or} \qquad \mathbf{C}^{(\mathrm{F})} = \frac{\mathrm{d}\boldsymbol{\sigma}^{(\mathrm{F})}}{\mathrm{d}\boldsymbol{\varepsilon}^{(\mathrm{Y})}} \tag{S1.15}$$

which can be expanded by using the spectral decomposition of $\boldsymbol{\sigma}^{(\mathrm{F})}$ [6]

$$\mathbf{C}^{(\mathrm{F})} = \sum_{i=1}^{3}\left\{\mathbf{E}_i \otimes \frac{\mathrm{d}\sigma_i^{(\mathrm{F})}}{\mathrm{d}\boldsymbol{\varepsilon}^{(\mathrm{Y})}} + \sigma_i^{(\mathrm{F})}\frac{\mathrm{d}\mathbf{E}_i}{\mathrm{d}\boldsymbol{\varepsilon}^{(\mathrm{Y})}}\right\} \tag{S1.16}$$

and applying the chain rule to its first term

$$\mathbf{C}^{(\mathrm{F})} = \sum_{i=1}^{3}\left\{\sum_{j=1}^{3}\left\{\frac{\partial\sigma_i^{(\mathrm{F})}}{\partial\varepsilon_j^{(\mathrm{Y})}}\mathbf{E}_i \otimes \frac{\mathrm{d}\varepsilon_j^{(\mathrm{Y})}}{\mathrm{d}\boldsymbol{\varepsilon}^{(\mathrm{Y})}} + \sigma_i^{(\mathrm{F})}\frac{\mathrm{d}\mathbf{E}_i}{\mathrm{d}\boldsymbol{\varepsilon}^{(\mathrm{Y})}}\right\}\right\} \tag{S1.17}$$

If $\varepsilon_{ij}^{(\mathrm{Y})}$ has three distinct eigenvalues ($\varepsilon_1^{(\mathrm{Y})} \neq \varepsilon_2^{(\mathrm{Y})} \neq \varepsilon_3^{(\mathrm{Y})}$), by taking the derivatives of $\varepsilon_j^{(\mathrm{Y})}$ and $\mathbf{E}_i$ with respect to $\boldsymbol{\varepsilon}^{(\mathrm{Y})}$, $\mathbf{C}^{(\mathrm{F})}$ can be derived as follows

$$\mathbf{C}^{(\mathrm{F})} = \sum_{a=1}^{3} \frac{\sigma_a^{(\mathrm{F})}}{(\varepsilon_a^{(\mathrm{Y})} - \varepsilon_b^{(\mathrm{Y})})(\varepsilon_a^{(\mathrm{Y})} - \varepsilon_c^{(\mathrm{Y})})} \left\{ \frac{\mathrm{d}\left(\boldsymbol{\varepsilon}^{(\mathrm{Y})}\right)^2}{\mathrm{d}\boldsymbol{\varepsilon}^{(\mathrm{Y})}} - \left(\varepsilon_b^{(\mathrm{Y})} + \varepsilon_c^{(\mathrm{Y})}\right)\mathbf{I}_{\mathrm{S}} \right.$$
$$- \left[\left(\varepsilon_a^{(\mathrm{Y})} - \varepsilon_b^{(\mathrm{Y})}\right) + \left(\varepsilon_a^{(\mathrm{Y})} - \varepsilon_c^{(\mathrm{Y})}\right)\right] \mathbf{E}_a \otimes \mathbf{E}_a$$
$$\left. - \left(\varepsilon_b^{(\mathrm{Y})} - \varepsilon_c^{(\mathrm{Y})}\right)(\mathbf{E}_b \otimes \mathbf{E}_b - \mathbf{E}_c \otimes \mathbf{E}_c) \right\} + \sum_{i=1}^{3}\sum_{j=1}^{3} \frac{\partial \sigma_i^{(\mathrm{F})}}{\partial \varepsilon_j^{(\mathrm{Y})}} \mathbf{E}_i \otimes \mathbf{E}_j \qquad \text{(S1.18)}$$

where the fourth-order tensor $\mathrm{d}\left(\boldsymbol{\varepsilon}^{(\mathrm{Y})}\right)^2/\mathrm{d}\boldsymbol{\varepsilon}^{(\mathrm{Y})}$ and $\mathbf{I}_{\mathrm{S}}$ (the fourth-order symmetric identity tensor) are obtained as follows

$$\left(\frac{\mathrm{d}\left(\boldsymbol{\varepsilon}^{(\mathrm{Y})}\right)^2}{\mathrm{d}\boldsymbol{\varepsilon}^{(\mathrm{Y})}}\right)_{ijkl} = \frac{1}{2}\left(\delta_{ik}\varepsilon_{lj}^{(\mathrm{Y})} + \delta_{il}\varepsilon_{kj}^{(\mathrm{Y})} + \delta_{jl}\varepsilon_{ik}^{(\mathrm{Y})} + \delta_{kj}\varepsilon_{il}^{(\mathrm{Y})}\right) \qquad \text{(S1.19)}$$

$$(\mathbf{I}_{\mathrm{S}})_{ijkl} = \frac{1}{2}\left(\delta_{ik}\delta_{jl} + \delta_{il}\delta_{jk}\right) \qquad \text{(S1.20)}$$

If $\varepsilon_{ij}^{(\mathrm{Y})}$ has two identical eigenvalues ($\varepsilon_1^{(\mathrm{Y})} \neq \varepsilon_2^{(\mathrm{Y})} = \varepsilon_3^{(\mathrm{Y})}$), then $\mathbf{C}^{(\mathrm{F})}$ is obtained as follows

$$\mathbf{C}^{(\mathrm{F})} = s_1 \frac{\mathrm{d}\left(\boldsymbol{\varepsilon}^{(\mathrm{Y})}\right)^2}{\mathrm{d}\boldsymbol{\varepsilon}^{(\mathrm{Y})}} - s_2\mathbf{I}_{\mathrm{S}} - s_3\boldsymbol{\varepsilon}^{(\mathrm{Y})} \otimes \boldsymbol{\varepsilon}^{(\mathrm{Y})} + s_4\boldsymbol{\varepsilon}^{(\mathrm{Y})} \otimes \mathbf{I} + s_5\mathbf{I} \otimes \boldsymbol{\varepsilon}^{(\mathrm{Y})} - s_6\mathbf{I} \otimes \mathbf{I} \qquad \text{(S1.21)}$$

where $\mathbf{I}$ is the second-order identity tensor

$$\mathrm{I}_{ij} = \delta_{ij} \qquad \text{(S1.22)}$$

and the constants s_1, s_2, s_3, s_4, s_5, and s_6 are given as follows

$$s_1 = \frac{\sigma_a^{(\mathrm{F})} - \sigma_c^{(\mathrm{F})}}{\left(\varepsilon_a^{(\mathrm{Y})} - \varepsilon_c^{(\mathrm{Y})}\right)^2} + \frac{1}{\varepsilon_a^{(\mathrm{Y})} - \varepsilon_c^{(\mathrm{Y})}}\left(\frac{\partial \sigma_c^{(\mathrm{F})}}{\partial \varepsilon_b^{(\mathrm{Y})}} - \frac{\partial \sigma_c^{(\mathrm{F})}}{\partial \varepsilon_c^{(\mathrm{Y})}}\right) \qquad \text{(S1.23a)}$$

$$s_2 = 2\varepsilon_c^{(\mathrm{Y})} \frac{\sigma_a^{(\mathrm{F})} - \sigma_c^{(\mathrm{F})}}{\left(\varepsilon_a^{(\mathrm{Y})} - \varepsilon_c^{(\mathrm{Y})}\right)^2} + \frac{\varepsilon_a^{(\mathrm{Y})} + \varepsilon_c^{(\mathrm{Y})}}{\varepsilon_a^{(\mathrm{Y})} - \varepsilon_c^{(\mathrm{Y})}} \left(\frac{\partial \sigma_c^{(\mathrm{F})}}{\partial \varepsilon_b^{(\mathrm{Y})}} - \frac{\partial \sigma_c^{(\mathrm{F})}}{\partial \varepsilon_c^{(\mathrm{Y})}} \right) \tag{S1.23b}$$

$$s_3 = 2 \frac{\sigma_a^{(\mathrm{F})} - \sigma_c^{(\mathrm{F})}}{\left(\varepsilon_a^{(\mathrm{Y})} - \varepsilon_c^{(\mathrm{Y})}\right)^3} + \frac{1}{\left(\varepsilon_a^{(\mathrm{Y})} - \varepsilon_c^{(\mathrm{Y})}\right)^2} \left(\frac{\partial \sigma_a^{(\mathrm{F})}}{\partial \varepsilon_c^{(\mathrm{Y})}} + \frac{\partial \sigma_c^{(\mathrm{F})}}{\partial \varepsilon_a^{(\mathrm{Y})}} - \frac{\partial \sigma_a^{(\mathrm{F})}}{\partial \varepsilon_a^{(\mathrm{Y})}} - \frac{\partial \sigma_c^{(\mathrm{F})}}{\partial \varepsilon_c^{(\mathrm{Y})}} \right) \tag{S1.23c}$$

$$\begin{aligned} s_4 = {} & 2\varepsilon_c^{(\mathrm{Y})} \frac{\sigma_a^{(\mathrm{F})} - \sigma_c^{(\mathrm{F})}}{\left(\varepsilon_a^{(\mathrm{Y})} - \varepsilon_c^{(\mathrm{Y})}\right)^3} + \frac{1}{\varepsilon_a^{(\mathrm{Y})} - \varepsilon_c^{(\mathrm{Y})}} \left(\frac{\partial \sigma_a^{(\mathrm{F})}}{\partial \varepsilon_c^{(\mathrm{Y})}} - \frac{\partial \sigma_c^{(\mathrm{F})}}{\partial \varepsilon_b^{(\mathrm{Y})}} \right) \\ & + \frac{\varepsilon_c^{(\mathrm{Y})}}{\left(\varepsilon_a^{(\mathrm{Y})} - \varepsilon_c^{(\mathrm{Y})}\right)^2} \left(\frac{\partial \sigma_a^{(\mathrm{F})}}{\partial \varepsilon_c^{(\mathrm{Y})}} + \frac{\partial \sigma_c^{(\mathrm{F})}}{\partial \varepsilon_a^{(\mathrm{Y})}} - \frac{\partial \sigma_a^{(\mathrm{F})}}{\partial \varepsilon_a^{(\mathrm{Y})}} - \frac{\partial \sigma_c^{(\mathrm{F})}}{\partial \varepsilon_c^{(\mathrm{Y})}} \right) \end{aligned} \tag{S1.23d}$$

$$\begin{aligned} s_5 = {} & 2\varepsilon_c^{(\mathrm{Y})} \frac{\sigma_a^{(\mathrm{F})} - \sigma_c^{(\mathrm{F})}}{\left(\varepsilon_a^{(\mathrm{Y})} - \varepsilon_c^{(\mathrm{Y})}\right)^3} + \frac{1}{\varepsilon_a^{(\mathrm{Y})} - \varepsilon_c^{(\mathrm{Y})}} \left(\frac{\partial \sigma_c^{(\mathrm{F})}}{\partial \varepsilon_a^{(\mathrm{Y})}} - \frac{\partial \sigma_c^{(\mathrm{F})}}{\partial \varepsilon_b^{(\mathrm{Y})}} \right) \\ & + \frac{\varepsilon_c^{(\mathrm{Y})}}{\left(\varepsilon_a^{(\mathrm{Y})} - \varepsilon_c^{(\mathrm{Y})}\right)^2} \left(\frac{\partial \sigma_a^{(\mathrm{F})}}{\partial \varepsilon_c^{(\mathrm{Y})}} + \frac{\partial \sigma_c^{(\mathrm{F})}}{\partial \varepsilon_a^{(\mathrm{Y})}} - \frac{\partial \sigma_a^{(\mathrm{F})}}{\partial \varepsilon_a^{(\mathrm{Y})}} - \frac{\partial \sigma_c^{(\mathrm{F})}}{\partial \varepsilon_c^{(\mathrm{Y})}} \right) \end{aligned} \tag{S1.23e}$$

$$\begin{aligned} s_6 = {} & 2\varepsilon_c^{(\mathrm{Y})} \frac{\sigma_a^{(\mathrm{F})} - \sigma_c^{(\mathrm{F})}}{\left(\varepsilon_a^{(\mathrm{Y})} - \varepsilon_c^{(\mathrm{Y})}\right)^3} + \frac{\varepsilon_a^{(\mathrm{Y})} \varepsilon_c^{(\mathrm{Y})}}{\left(\varepsilon_a^{(\mathrm{Y})} - \varepsilon_c^{(\mathrm{Y})}\right)^2} \left(\frac{\partial \sigma_a^{(\mathrm{F})}}{\partial \varepsilon_c^{(\mathrm{Y})}} + \frac{\partial \sigma_c^{(\mathrm{F})}}{\partial \varepsilon_a^{(\mathrm{Y})}} \right) - \frac{\left(\varepsilon_c^{(\mathrm{Y})}\right)^2}{\left(\varepsilon_a^{(\mathrm{Y})} - \varepsilon_c^{(\mathrm{Y})}\right)^2} \left(\frac{\partial \sigma_a^{(\mathrm{F})}}{\partial \varepsilon_a^{(\mathrm{Y})}} + \frac{\partial \sigma_c^{(\mathrm{F})}}{\partial \varepsilon_c^{(\mathrm{Y})}} \right) \\ & - \frac{\varepsilon_a^{(\mathrm{Y})} + \varepsilon_c^{(\mathrm{Y})}}{\varepsilon_a^{(\mathrm{Y})} - \varepsilon_c^{(\mathrm{Y})}} \frac{\partial \sigma_c^{(\mathrm{F})}}{\partial \varepsilon_b^{(\mathrm{Y})}} \end{aligned} \tag{S1.23f}$$

where (a, b, c) are here cyclic permutations of (1,2,3).

Finally, if $\varepsilon_{ij}^{(\mathrm{Y})}$ has three identical eigenvalues ($\varepsilon_1^{(\mathrm{Y})} = \varepsilon_2^{(\mathrm{Y})} = \varepsilon_3^{(\mathrm{Y})}$), then $\mathbf{C}^{(\mathrm{F})}$ is given as follows

$$\mathbf{C}^{(\mathrm{F})} = \left(\frac{\partial \sigma_1^{(\mathrm{F})}}{\partial \varepsilon_1^{(\mathrm{Y})}} - \frac{\partial \sigma_1^{(\mathrm{F})}}{\partial \varepsilon_2^{(\mathrm{Y})}} \right) \mathbf{I}_{\mathrm{S}} + \frac{\partial \sigma_1^{(\mathrm{F})}}{\partial \varepsilon_2^{(\mathrm{Y})}} \mathbf{I} \otimes \mathbf{I} \tag{S1.24}$$

Note that $\partial \sigma_i^{(\mathrm{F})} / \partial \varepsilon_j^{(\mathrm{Y})}$ in equations (S1.18), (S1.23), and (S1.24) can be derived by taking the derivative of equation (S1.14)

$$\frac{\partial \sigma_i^{(\mathrm{F})}}{\partial \varepsilon_i^{(\mathrm{Y})}} = \frac{\partial}{\partial \varepsilon_i^{(\mathrm{Y})}}\left(\frac{\partial f}{\partial \varepsilon_i^{(\mathrm{Y})}}\right) = \begin{cases} 0 & \varepsilon_i^{(\mathrm{Y})} < \epsilon_1 \\ \ell\left[\dfrac{\left(\dfrac{\varepsilon_i^{(\mathrm{Y})} - \epsilon_1}{\epsilon_2 - \epsilon_1}\right)^t \left(\varepsilon_i^{(\mathrm{Y})} - \epsilon_1\right)}{t+1}\right] & \epsilon_1 \le \varepsilon_i^{(\mathrm{Y})} < \epsilon_2 \\ \ell\left[\dfrac{\left(1 + \varepsilon_i^{(\mathrm{Y})} - \epsilon_2\right)^{s+1} - 1}{s+1} + \dfrac{\epsilon_2 - \epsilon_1}{t+1}\right] & \varepsilon_i^{(\mathrm{Y})} \ge \epsilon_2 \end{cases} \tag{S1.25}$$

Also, note that $\sigma_i^{(\mathrm{F})}$ in our formulation is a function of $\varepsilon_i^{(\mathrm{Y})}$ only and there is no dependence of $\sigma_i^{(\mathrm{F})}$ on $\varepsilon_j^{(\mathrm{Y})}$ for $i \neq j$.

1.4. Total cytoskeletal stiffness

The cytoskeleton is composed of these three elements: (i) the myosin motors, (ii) the microtubules, and (iii) the actin filaments. As the actin element is connected in series to the other two elements (see Fig.S9), the total stiffness of the cell, $\mathbf{C}$, can be obtained as follows

$$\mathbf{C} = \left(\left(\mathbf{C}^{(\mathrm{X})}\right)^{-1} + \left(\mathbf{C}^{(\mathrm{Y})}\right)^{-1}\right)^{-1} \tag{S1.26a}$$

where

$$\mathbf{C}^{(\mathrm{X})} = \mathbf{C}^{(\rho)} + \mathbf{C}^{(\mathrm{MT})} \tag{S1.26b}$$

and

$$\mathbf{C}^{(\mathrm{Y})} = \mathbf{C}^{(\mathrm{A})} = \mathbf{C}^{(\mathrm{I})} + \mathbf{C}^{(\mathrm{F})} \tag{S1.26c}$$

In equation (S2.35), the second-order tensors $\mathbf{C}^{(\rho)}$, $\mathbf{C}^{(\mathrm{MT})}$, and $\mathbf{C}^{(\mathrm{A})}$ are the 6×6 matrix representations of the fourth-order tensors $\mathbf{C}^{(\rho)}$ (equation S1.7), $\mathbf{C}^{(\mathrm{MT})}$ (equation S1.4), and $\mathbf{C}^{(\mathrm{A})}$ (equation S1.8), respectively. Note that all the above fourth-order stiffness tensors can be degraded to square matrices to be used in the finite element framework. For example, the fourth-order tensor C_{ijkl} can be degraded to the second-order tensor C_{ij} as follows

$$\mathrm{C}_{ij} = \begin{bmatrix} \mathrm{C}_{1111} & \mathrm{C}_{1122} & \mathrm{C}_{1133} & \mathrm{C}_{1112} & \mathrm{C}_{1113} & \mathrm{C}_{1123} \\ \mathrm{C}_{2211} & \mathrm{C}_{2222} & \mathrm{C}_{2233} & \mathrm{C}_{2212} & \mathrm{C}_{2213} & \mathrm{C}_{2223} \\ \mathrm{C}_{3311} & \mathrm{C}_{3322} & \mathrm{C}_{3333} & \mathrm{C}_{3312} & \mathrm{C}_{3313} & \mathrm{C}_{3323} \\ \mathrm{C}_{1211} & \mathrm{C}_{1222} & \mathrm{C}_{1233} & \mathrm{C}_{1212} & \mathrm{C}_{1213} & \mathrm{C}_{1223} \\ \mathrm{C}_{1311} & \mathrm{C}_{1322} & \mathrm{C}_{1333} & \mathrm{C}_{1312} & \mathrm{C}_{1313} & \mathrm{C}_{1323} \\ \mathrm{C}_{2311} & \mathrm{C}_{2322} & \mathrm{C}_{2333} & \mathrm{C}_{2312} & \mathrm{C}_{2313} & \mathrm{C}_{2323} \end{bmatrix} \tag{S1.27}$$

1.5. The system of nonlinear equations

In our coarse-grained finite element model, the total cytoskeletal stress field σ_{ij} can be determined from (S1.5) or (S1.10). The total cytoskeletal stiffness C_{ij} can be also given by equation (S1.26). However, both σ_{ij} and C_{ij} are functions of unknown strain tensors $\varepsilon_{ij}^{(\mathrm{X})}$ and $\varepsilon_{ij}^{(\mathrm{Y})}$. Thus, using an iterative procedure, we first need to determine our unknowns strain tensors $\varepsilon_{ij}^{(\mathrm{X})}$ and $\varepsilon_{ij}^{(\mathrm{Y})}$. To this end, we first define the following 12×1 vector

$$\boldsymbol{u} = \{u_1 \quad u_2 \quad \cdots \quad u_{12}\}^{\mathrm{T}} \tag{S1.28a}$$

which contains our unknown variables

$$\boldsymbol{u} = \left\{\varepsilon_{11}^{(\mathrm{X})} \quad \varepsilon_{22}^{(\mathrm{X})} \quad \varepsilon_{33}^{(\mathrm{X})} \quad \varepsilon_{12}^{(\mathrm{X})} \quad \varepsilon_{13}^{(\mathrm{X})} \quad \varepsilon_{23}^{(\mathrm{X})} \quad \varepsilon_{11}^{(\mathrm{Y})} \quad \varepsilon_{22}^{(\mathrm{Y})} \quad \varepsilon_{33}^{(\mathrm{Y})} \quad \varepsilon_{12}^{(\mathrm{Y})} \quad \varepsilon_{13}^{(\mathrm{Y})} \quad \varepsilon_{23}^{(\mathrm{Y})}\right\}^{\mathrm{T}} \tag{S1.28b}$$

We then need 12 equations to determine these 12 unknowns and to define our system of equations. 6 of these 12 equations can be obtained from the following condition

$$\boldsymbol{\sigma} = \boldsymbol{\sigma}^{(\mathrm{X})} = \boldsymbol{\sigma}^{(\mathrm{Y})} \tag{S1.29}$$

where $\boldsymbol{\sigma}^{(\mathrm{X})}$ is the stress generated by the actomyosin contractility which is directly transmitted to the actin filament network (see equations (S1.5) and (S1.6))

$$\sigma_{ij}^{(\mathrm{X})} = \sigma_{ij} = \left(\mathrm{C}_{ijkl}^{(\rho)} + \mathrm{C}_{ijkl}^{(\mathrm{MT})}\right)\varepsilon_{kl}^{(\mathrm{X})} + \bar{\rho}_0\delta_{ij} \tag{S1.30}$$

and $\boldsymbol{\sigma}^{(\mathrm{Y})}$ is the stress transmitted to the actin filament network (see equation S1.10)

$$\sigma_{ij}^{(\mathrm{Y})} = \sigma_{ij} = \sigma_{ij}^{(\mathrm{A})} = \sigma_{ij}^{(\mathrm{I})} + \sigma_{ij}^{(\mathrm{F})} \tag{S1.31}$$

The other 6 equations can be obtained from the following condition

$$\boldsymbol{\varepsilon} = \boldsymbol{\varepsilon}^{(\mathrm{X})} + \boldsymbol{\varepsilon}^{(\mathrm{Y})} \tag{S1.32}$$

where the second-order tensor $\boldsymbol{\varepsilon}$ is the total strain of the cell. As both stress and strain tensors $\sigma_{ij}^{(\mathrm{X})}$, $\sigma_{ij}^{(\mathrm{Y})}$, $\varepsilon_{ij}^{(\mathrm{X})}$, and $\varepsilon_{ij}^{(\mathrm{Y})}$ are symmetric, we can define the 12×1 vector $\boldsymbol{f}$

$$\boldsymbol{f} = \{f_1 \quad f_2 \quad \dots \quad f_{12}\}^{\mathrm{T}} \tag{S1.33a}$$

which contains our 12 equations

$$f_1 = \sigma_{11}^{(\mathrm{X})} - \sigma_{11}^{(\mathrm{Y})} \tag{S1.33b}$$

$$f_2 = \sigma_{22}^{(\mathrm{X})} - \sigma_{22}^{(\mathrm{Y})} \tag{S1.33c}$$

$$f_3 = \sigma_{33}^{(\mathrm{X})} - \sigma_{33}^{(\mathrm{Y})} \tag{S1.33d}$$

$$f_4 = \sigma_{12}^{(\mathrm{X})} - \sigma_{12}^{(\mathrm{Y})} \tag{S1.33e}$$

$$f_5 = \sigma_{13}^{(\mathrm{X})} - \sigma_{13}^{(\mathrm{Y})} \tag{S1.33f}$$

$$f_6 = \sigma_{23}^{(\mathrm{X})} - \sigma_{23}^{(\mathrm{Y})} \tag{S1.33g}$$

$$f_7 = \varepsilon_{11} - \varepsilon_{11}^{(\mathrm{X})} - \varepsilon_{11}^{(\mathrm{Y})} \tag{S1.33h}$$

$$f_8 = \varepsilon_{22} - \varepsilon_{22}^{(\mathrm{X})} - \varepsilon_{22}^{(\mathrm{Y})} \tag{S1.33i}$$

$$f_9 = \varepsilon_{33} - \varepsilon_{33}^{(\mathrm{X})} - \varepsilon_{33}^{(\mathrm{Y})} \tag{S1.33j}$$

$$f_{10} = \varepsilon_{12} - \varepsilon_{12}^{(\mathrm{X})} - \varepsilon_{12}^{(\mathrm{Y})} \tag{S1.33k}$$

$$f_{11} = \varepsilon_{13} - \varepsilon_{13}^{(\mathrm{X})} - \varepsilon_{13}^{(\mathrm{Y})} \tag{S1.33l}$$

$$f_{12} = \varepsilon_{23} - \varepsilon_{23}^{(\mathrm{X})} - \varepsilon_{23}^{(\mathrm{Y})} \tag{S1.33m}$$

We then determine the 12×12 Jacobian matrix **J**

$$\mathbf{J}=\begin{bmatrix} \partial f_1/\partial u_1 & \partial f_1/\partial u_2 & \dots & \partial f_1/\partial u_{12} \\ \partial f_2/\partial u_1 & \partial f_2/\partial u_2 & \dots & \partial f_2/\partial u_{12} \\ \vdots & \vdots & & \vdots \\ . & . & & . \\ \partial f_{12}/\partial u_1 & \partial f_{12}/\partial u_2 & \dots & \partial f_{12}/\partial u_{12} \end{bmatrix}=\begin{bmatrix} \mathbf{C}^{(\mathrm{X})} & -\mathbf{C}^{(\mathrm{Y})} \\ -\mathbf{I} & -\mathbf{I} \end{bmatrix} \tag{S1.34}$$

which is used in the Newton-Raphson method to determine the unknown vector $\boldsymbol{u}$

$$\boldsymbol{u}_{i+1}=\boldsymbol{u}_i-\mathbf{J}^{-1}\boldsymbol{f}(\boldsymbol{u}_i) \tag{S1.35}$$

where $\boldsymbol{u}_i$ and $\boldsymbol{u}_{i+1}$ are respectively the solutions for i and $i+1$ iterations. The following initial guess $\boldsymbol{u}_0$ and convergence criterion are used in our simulations

$$\boldsymbol{u}_0=\{0 \quad 0 \quad \dots \quad 0\}^{\mathrm{T}}_{1\times 12} \tag{S1.36}$$

$$|\boldsymbol{f}|=\sqrt{(f_1)^2+(f_2)^2+\cdots+(f_{12})^2}<\epsilon_{\mathrm{Tol}} \tag{S1.37}$$

where ϵ_{Tol} is the convergence threshold. Using $\epsilon_{\mathrm{Tol}}=10^{-8}$ in our simulations, we stop the iterative process (S1.35) when the magnitude of the vector $\boldsymbol{f}$ is less than ϵ_{Tol}. With $\varepsilon_{ij}^{(\mathrm{X})}$ and $\varepsilon_{ij}^{(\mathrm{Y})}$ obtained from (S1.35), we can calculate the total cytoskeletal stress field σ_{ij} from equations (S1.30) or (S1.31) and the total cytoskeletal stiffness C_{ij} from equation (S1.26) to complete our constitutive equations.

1.6. Actomyosin contractility increases with tension anisotropy

Combining equation (S1.5) with (S1.6), it can be shown that the average of contractility, $\frac{1}{3}\rho_{kk}=(\rho_{11}+\rho_{22}+\rho_{33})/3$, increases with the average of stress, $\frac{1}{3}\sigma_{kk}=(\sigma_{11}+\sigma_{22}+\sigma_{33})/3$, [1,7]

$$\frac{\rho_{kk}}{3}=\left(\frac{3K^{(\mathrm{MT})}\alpha_{\mathrm{v}}-1}{3K^{(\mathrm{MT})}\beta_{\mathrm{v}}-1}\right)\frac{\sigma_{kk}}{3}+\left(\frac{3K^{(\mathrm{MT})}\beta_{\mathrm{v}}}{3K^{(\mathrm{MT})}\beta_{\mathrm{v}}-1}\right)\rho_0 \tag{S1.38}$$

The above feedback between the averages of contractility and stress enables us to capture the fact that actomyosin contractility increases with cell substrate area [8] and microenvironment stiffness [5,9]. However, actomyosin contractility has been also observed to increase with cell

polarization [8] where fibroblasts cultured on a rectangular substrate (anisotropic tension) have higher levels of phosphorylated myosin light chain (a marker for myosin II contractility) and F-actin compared to fibroblasts cultured on a square substrate (isotropic tension) with the same substrate area [8]. To capture the fact that contractility increases with anisotropy in the components of the stress tensor σ_{ij}, equation (S1.38) is modified as follows

$$\frac{\rho_{kk}}{3} = \left(\frac{3K^{(\mathrm{MT})}\alpha_{\mathrm{v}} - 1}{3K^{(\mathrm{MT})}\beta_{\mathrm{v}} - 1}\right)\frac{\sigma_{kk}}{3} + \alpha_{\mathrm{a}}\sigma_{\mathrm{a}} + \left(\frac{3K^{(\mathrm{MT})}\beta_{\mathrm{v}}}{3K^{(\mathrm{MT})}\beta_{\mathrm{v}} - 1}\right)\rho_0 \tag{S1.39}$$

where $\sigma_{\mathrm{a}} = \tanh\left(\frac{1}{2}\left(\frac{\sigma_1}{\sigma_2} - 1\right)\right)\sigma_1$ represents the anisotropy in tension (stress polarization) while $\sigma_1 > \sigma_2 > \sigma_3$ are the principal stress values of the stress tensor σ_{ij} with $\sigma_1 > \sigma_2 > 0$. Also, α_{a} in the above equation is the anisotropic chemo-mechanical feedback parameter which regulates the increase in myosin phosphorylation with anisotropic tension. To implement equation (S1.39) in our finite element framework, we use a piecewise linear approximation and we simply replace ρ_0 in equation (S1.3) with $\rho_0 + \left(\frac{3K^{(\mathrm{MT})}\beta_{\mathrm{v}} - 1}{3K^{(\mathrm{MT})}\beta_{\mathrm{v}}}\right)\alpha_{\mathrm{a}}\sigma_{\mathrm{a}}$ in each step of the simulation. Note that replacing $\left(\frac{3K^{(\mathrm{MT})}\alpha_{\mathrm{v}} - 1}{3K^{(\mathrm{MT})}\beta_{\mathrm{v}} - 1}\right)$, α_{a}, and $\left(\frac{3K^{(\mathrm{MT})}\beta_{\mathrm{v}}}{3K^{(\mathrm{MT})}\beta_{\mathrm{v}} - 1}\right)$ in equation (S1.39) with f_{m}, f_{a}, and f_0, respectively, gives us equation (1) in the main text.

2. Nuclear Interior (Chromatin)

Recent uniaxial stretching experiments of single isolated nuclei shows that, unlike the lamin network, chromatin does not exhibit strain stiffening even at large extensions [10]. Therefore, we model chromatin as a linear elastic material [1]

$$\bar{\sigma}_{ij} = \bar{\mathrm{C}}_{ijkl}\,\bar{\varepsilon}_{kl} = \frac{\bar{E}}{3(1 - 2\bar{\nu})}\delta_{ij}\bar{\varepsilon}_{kk} + \frac{\bar{E}}{(1 + \bar{\nu})}\left(\bar{\varepsilon}_{ij} - \frac{1}{3}\delta_{ij}\bar{\varepsilon}_{kk}\right) \tag{S2.1}$$

where $\bar{\boldsymbol{\sigma}}$ and $\bar{\boldsymbol{\varepsilon}}$ are respectively the second-order stress and strain tensors in the chromatin model, and $\bar{\mathbf{C}}$ is the fourth-order stiffness tensor of chromatin

[1] All tensors, vectors, and scalars used in the chromatin model are denoted by "‾".

$$\bar{\mathrm{C}}_{ijkl} = \bar{K}\delta_{ij}\delta_{kl} + \bar{\mu}\left(\delta_{ik}\delta_{jk} + \delta_{il}\delta_{jk} - \frac{2}{3}\delta_{ij}\delta_{kl}\right) \tag{S2.2a}$$

with

$$\bar{K} = \frac{\bar{E}}{3(1-2\bar{v})} \quad , \quad \bar{\mu} = \frac{\bar{E}}{2(1+\bar{v})} \tag{S2.2b}$$

where $\bar{K}$, $\bar{\mu}$, $\bar{E}$, and $\bar{v}$ are the bulk modulus, shear modulus, elastic modulus, and Poisson's ratio of chromatin, respectively. In addition to chromatin, the nuclear interior is also filled with fluid which causes hydrostatic pressure as the nucleus is deformed by contractility-dependent compressive forces.

3. Nuclear Envelope

Consistent with the experimentally observed fibrous nature of the lamina of the mammalian cell nuclei [11], the nuclear envelope is modeled as a filamentous network material (lamin network) which stiffens with tension. To this end, we first decompose the stress in the nuclear envelope $\hat{\sigma}_{ij}$ as follows [2]

$$\hat{\sigma}_{ij} = \hat{\sigma}_{ij}^{(\mathrm{I})} + \hat{\sigma}_{ij}^{(\mathrm{F})} \tag{S3.1}$$

where $\hat{\boldsymbol{\sigma}}^{(\mathrm{I})}$ is linearly related to the nuclear envelope strain $\hat{\boldsymbol{\varepsilon}}$ using the initial stiffness of the nuclear envelope, $\hat{\mathbf{C}}^{(\mathrm{I})}$,

$$\hat{\sigma}_{ij}^{(\mathrm{I})} = \hat{\mathrm{C}}_{ijkl}^{(\mathrm{I})}\,\hat{\varepsilon}_{kl} \tag{S3.2}$$

while $\hat{\boldsymbol{\sigma}}^{(\mathrm{F})}$ is a nonlinear function of the strain tensor $\hat{\boldsymbol{\varepsilon}}$

$$\hat{\boldsymbol{\sigma}}^{(\mathrm{F})} = \sum_{i=1}^{3} \frac{\partial \hat{f}(\hat{\varepsilon}_i)}{\partial \hat{\varepsilon}_i} \hat{\boldsymbol{n}}_i \otimes \hat{\boldsymbol{n}}_i = \sum_{i=1}^{3} \hat{\sigma}^{(\mathrm{F})}(\hat{\varepsilon}_i)\,\hat{\mathbf{E}}_i = \sum_{i=1}^{3} \hat{\sigma}_i^{(\mathrm{F})}\,\hat{\mathbf{E}}_i \tag{S3.3}$$

where the orthogonal eigenvectors $\hat{\boldsymbol{n}}_1$, $\hat{\boldsymbol{n}}_2$, and $\hat{\boldsymbol{n}}_3$ are the unit vectors in the directions of the principal strains $\hat{\varepsilon}_1$, $\hat{\varepsilon}_2$, and $\hat{\varepsilon}_3$, respectively, and the symmetric tensors $\hat{\mathbf{E}}_1 = \hat{\boldsymbol{n}}_1 \otimes \hat{\boldsymbol{n}}_1$, $\hat{\mathbf{E}}_2 =$

[2] All tensors, vectors, and scalars used in the nuclear envelope model are denoted by "^".

$\hat{\boldsymbol{n}}_2 \otimes \hat{\boldsymbol{n}}_2$, and $\hat{\mathbf{E}}_3 = \hat{\boldsymbol{n}}_3 \otimes \hat{\boldsymbol{n}}_3$ are the eigenprojections of the strain tensor $\hat{\boldsymbol{\varepsilon}}$. Note that $\otimes$ in equation (S3.3) represents the dyadic product of two arbitrary vectors $\boldsymbol{u}$ and $\boldsymbol{v}$ as $(\boldsymbol{u} \otimes \boldsymbol{v})_{ij} = u_i v_j$. As shown in (S3.3), the stress tensor $\hat{\boldsymbol{\sigma}}^{(\mathrm{F})}$ is defined as a function of its eigenprojections ($\hat{\mathbf{E}}_1$, $\hat{\mathbf{E}}_2$, $\hat{\mathbf{E}}_3$) and principal stresses ($\hat{\sigma}_1^{(\mathrm{F})}$, $\hat{\sigma}_2^{(\mathrm{F})}$, $\hat{\sigma}_3^{(\mathrm{F})}$). The eigenprojections $\hat{\mathbf{E}}_1$, $\hat{\mathbf{E}}_2$, and $\hat{\mathbf{E}}_3$ can be determined from the following spectral decomposition of the strain tensor $\hat{\boldsymbol{\varepsilon}}$

$$\hat{\boldsymbol{\varepsilon}} = \sum_{i=1}^{3} \hat{\varepsilon}_i \, \hat{\boldsymbol{n}}_i \otimes \hat{\boldsymbol{n}}_i = \sum_{i=1}^{3} \hat{\varepsilon}_i \, \hat{\mathbf{E}}_i \tag{S3.4}$$

We use equation (S1.14) to define the principal stresses ($\hat{\sigma}_1^{(\mathrm{F})}$, $\hat{\sigma}_2^{(\mathrm{F})}$, $\hat{\sigma}_3^{(\mathrm{F})}$) as functions of the principal strains ($\hat{\varepsilon}_1$, $\hat{\varepsilon}_2$, $\hat{\varepsilon}_3$) which have been previously determined from equation (S3.4)

$$\hat{\sigma}_i^{(\mathrm{F})} = \frac{\partial \hat{f}(\hat{\varepsilon}_i)}{\partial \hat{\varepsilon}_i} = \tag{S3.5}$$

$$\begin{cases} 0 & \hat{\varepsilon}_i < \hat{\epsilon}_1 \\ \hat{\ell}\left[\dfrac{\left(\dfrac{\hat{\varepsilon}_i - \hat{\epsilon}_1}{\hat{\epsilon}_2 - \hat{\epsilon}_1}\right)^{\hat{n}} (\hat{\varepsilon}_i - \hat{\epsilon}_1)^2}{(\hat{n}+1)(\hat{n}+2)}\right] & \hat{\epsilon}_1 \le \hat{\varepsilon}_i < \hat{\epsilon}_2 \\ \hat{\ell}\left[\dfrac{(1+\hat{\varepsilon}_i - \hat{\epsilon}_2)^{\hat{m}+2} - 1}{(\hat{m}+1)(\hat{m}+2)} + \dfrac{\hat{\epsilon}_2 - \hat{\varepsilon}_i}{\hat{m}+1} + \dfrac{(\hat{\varepsilon}_i - \hat{\epsilon}_2)(\hat{\epsilon}_2 - \hat{\epsilon}_1)}{\hat{n}+1} + \dfrac{(\hat{\epsilon}_2 - \hat{\epsilon}_1)^2}{(\hat{n}+1)(\hat{n}+2)}\right] & \hat{\varepsilon}_i \ge \hat{\epsilon}_2 \end{cases}$$

In the above equation, $\hat{\epsilon}_1 = \hat{\epsilon}_{\mathrm{c}} - 0.5\hat{\epsilon}_{\mathrm{t}}$ and $\hat{\epsilon}_2 = \hat{\epsilon}_{\mathrm{c}} + 0.5\hat{\epsilon}_{\mathrm{t}}$ are the transition points, $\hat{\epsilon}_{\mathrm{t}} = 0.25\hat{\epsilon}_{\mathrm{c}}$ is the transition width, $\hat{\epsilon}_{\mathrm{c}}$ is the critical (tensile) principal strain, $\hat{n}$ is the transition constant, and $\hat{\ell}$ and $\hat{m}$ are the stiffening parameters which regulate strain stiffening of the lamin network at large strains $\hat{\varepsilon}_i \ge \hat{\epsilon}_2$.

Similar to equation (S3.1), the stiffness of the nuclear envelope lamina network $\widehat{\mathbf{C}}$ can be decomposed as follows

$$\widehat{\mathrm{C}}_{ijkl} = \widehat{\mathrm{C}}_{ijkl}^{(\mathrm{I})} + \widehat{\mathrm{C}}_{ijkl}^{(\mathrm{F})} \tag{S3.6}$$

where $\widehat{\mathbf{C}}^{(\mathrm{I})}$ is the initial stiffness of the nuclear envelope lamina network

$$\widehat{\mathrm{C}}_{ijkl}^{(\mathrm{I})} = \widehat{K}^{(\mathrm{I})}\delta_{ij}\delta_{kl} + \hat{\mu}^{(\mathrm{I})}\left(\delta_{ik}\delta_{jk} + \delta_{il}\delta_{jk} - \frac{2}{3}\delta_{ij}\delta_{kl}\right) \tag{S3.7}$$

and $\widehat{K}^{(\mathrm{I})}$ and $\hat{\mu}^{(\mathrm{I})}$ are respectively the initial bulk and shear moduli of the lamin network. The second term in equation (S3.6) captures the tension stiffening of the nuclear lamina network and can be calculated using the following piecewise linear approximation

$$\widehat{\mathrm{C}}_{ijkl}^{(\mathrm{F})} = \frac{\mathrm{d}\hat{\sigma}_{ij}^{(\mathrm{F})}}{\mathrm{d}\hat{\varepsilon}_{kl}} \tag{S3.8}$$

Similar to equation (S1.15), the exact expression for $\widehat{\mathrm{C}}_{ijkl}^{(\mathrm{F})}$ can be determined from equations (S1.16-25) by replacing $\sigma_i^{(\mathrm{F})}$, $\varepsilon_i^{(\mathrm{Y})}$, $\mathbf{E}_i$, and $\boldsymbol{\varepsilon}^{(\mathrm{Y})}$ with $\hat{\sigma}_i^{(\mathrm{F})}$, $\hat{\varepsilon}_i$, $\hat{\mathbf{E}}_i$, and $\hat{\boldsymbol{\varepsilon}}$, respectively ($i = 1, 2, 3$).

Table S1: Comparison between literature data and this work on lamin A/C knockdown (KD)

No.	Relative change of Young's modulus	Method	Cell line	Nucleus status	Treatment protocol	References*
1	-33%	Micropipette aspiration	Mouse embryonic fibroblasts	Intact nucleus	Gene silencing, 100% KD	Ref.4
2	-55%	Micropipette aspiration	A549	Intact nucleus	siRNA transfection, >85% KD	Ref.22
3	-65.6%	Micropipette aspiration	A549	Isolated nucleus	siRNA transfection	Ref.7
4	-46%	Micropipette aspiration	Mesenchymal stem cells	Isolated nucleus	siRNA transfection	Ref.7
5	-55.7%	Membranes-induced strain	Mouse skeletal myoblasts	Intact nucleus	Gene silencing, 100% KD	Ref.24
6	-48%	Micropipette aspiration	A549	Intact nucleus	siRNA transfection, 50% KD	Ref.25
7	-36%	Pipette-based micromanipulation	HeLa	Isolated nucleus	siRNA transfection, 80% KD	Ref.26
8	-24%	Brillouin	NIH 3T3	Intact nucleus	siRNA transfection, 66% KD	This work

* the references in the main text.

Table S2: Comparison between literature data and this work on chromatin decondensation

No.	Relative change of Young's modulus	Method	Cell line	Nucleus status	Treatment protocol	References*
1	-33%	Optical stretcher	Mouse embryonic stem cell	Intact nucleus	90 ng/mL, 2 hours	Ref.30
2	-56%	AFM	Cardiac myocytes	Intact nucleus	200 μg/mL, 4 hours	Ref.29
3	-26%	AFM	human HT1080 fibrosarcoma	Intact nucleus	100 ng/mL, 24 hours	Ref.28
4	-30%	Micropipette-based micromanipulation	Mouse embryonic fibroblasts	Isolated nucleus	30 ng/mL, 16-24 hours	Ref.26
5	-32%	Micropipette-based micromanipulation	HeLa	Isolated nucleus	30 ng/mL, 16-24 hours	Ref.26
6	-53.5%	Microneedle-based micromanipulation	HeLa	Isolated nucleus	150 ng/mL, 3 hours	Ref.31
7	-27%	Brillouin	NIH 3T3	Intact nucleus	100 ng/mL, 2 hours	This work

* the references in the main text.

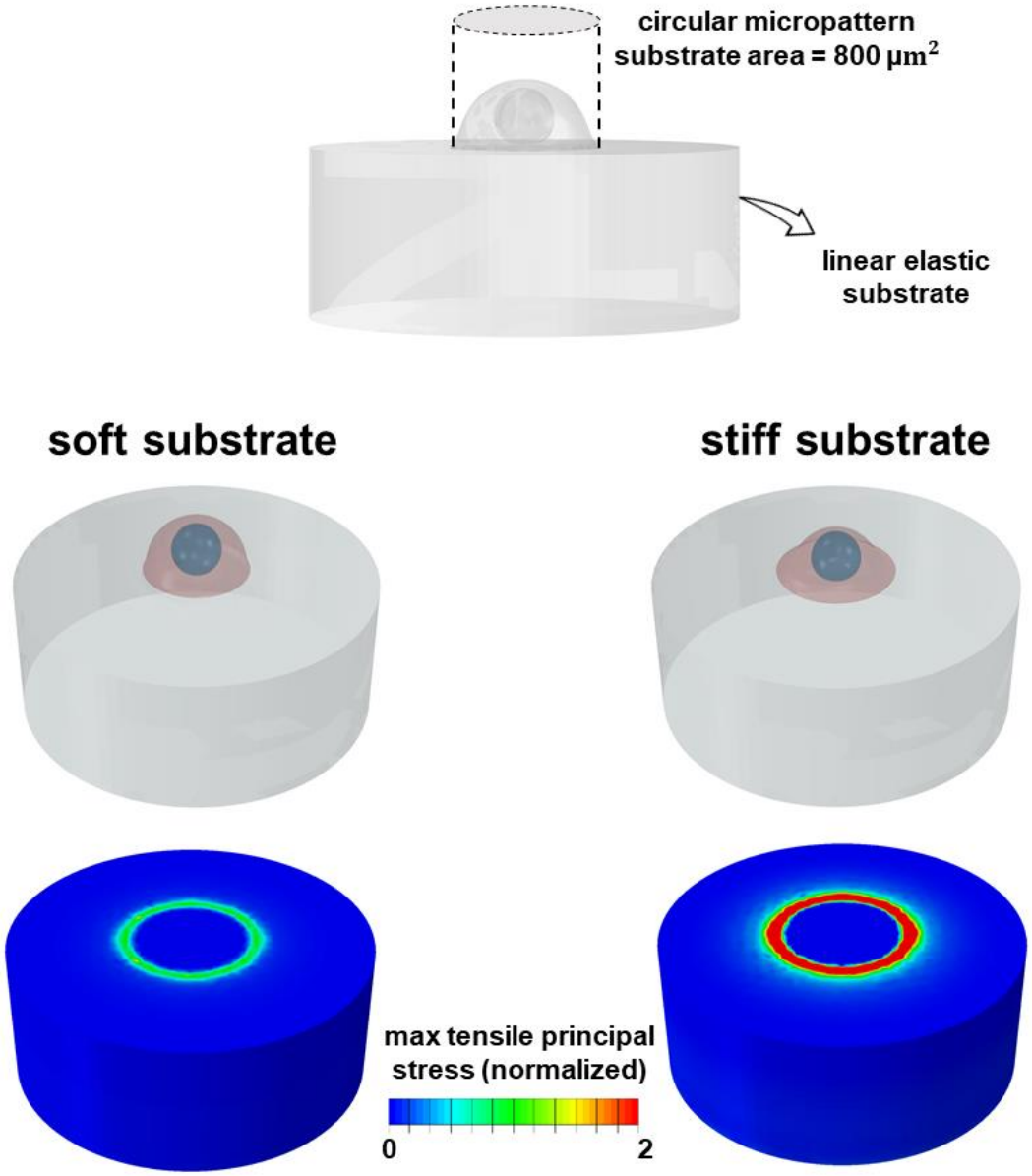

Fig. S1. Cell traction force, cell stiffness, and actomyosin contractility increases with substrate stiffness. NIH 3T3 fibroblasts are cultured on circular micropatterned substrates with different substrate stiffness [12]. The model predicts that cells on stiffer substrates generate higher tractions forces which is in agreement with traction force microscopy results in reference [12]. Furthermore, the cell contractility, ρ_{ij}, the stiffness of the actin network, $C_{ijkl}^{(A)}$, and the stress it carries, σ_{ij}, increase with substrate stiffness in our simulations while nuclear height decreases with increasing substrate stiffness.

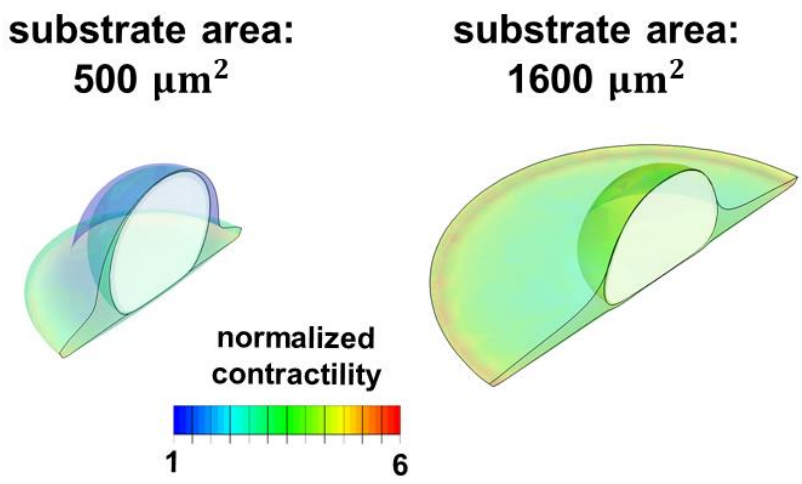

Fig. S2. Cell traction force, cell stiffness, and actomyosin contractility increases with substrate area. NIH 3T3 fibroblasts are cultured on rigid circular micropatterned substrates with different substrate areas [8]. Our simulations demonstrate the maximum principal contractility $\rho_{\max} = \rho_1 > \rho_2 > \rho_3$ for cells with small and large substrates where ρ_1, ρ_2, and ρ_3 are the eigenvalues of the contractility tensor ρ_{ij}. The model predicts that cells on larger substrates exhibit higher contractility which is in agreement with experimental observations in reference [8] where cells with higher substrate areas have higher levels of phosphorylated myosin light chain (p-MLC). Also, similar to the effect of substrate stiffness in Supplementary Fig.1, the stiffness of the actin network, $C_{ijkl}^{(A)}$, and the stress it carries, σ_{ij}, increase with substrate area in our simulations while nuclear height decreases with increasing substrate area.

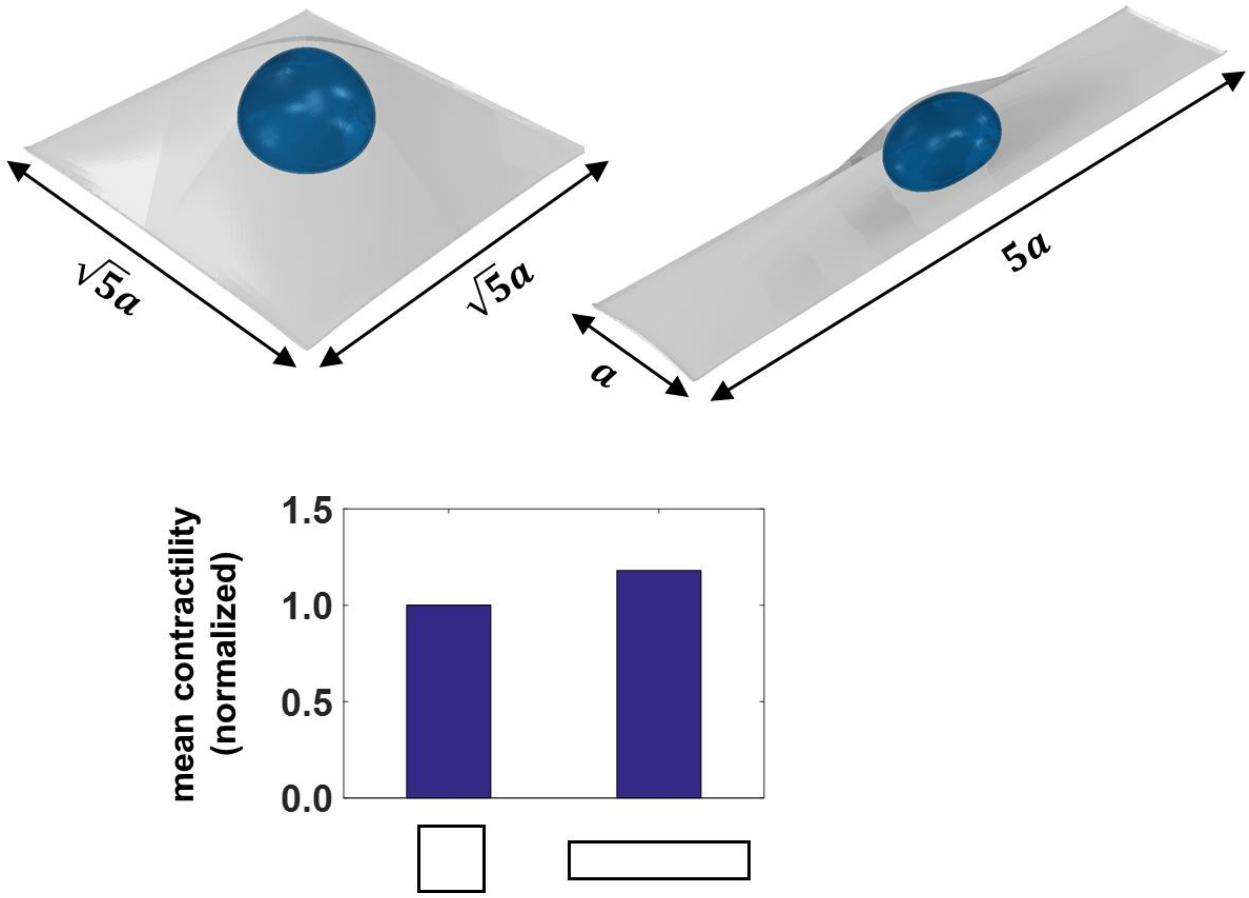

Fig. S3. Actomyosin contractility increases with substrate aspect ratio. NIH 3T3 fibroblasts are cultured on rigid micropatterned substrates with the same surface area but different substrate aspect ratios [13]. Our simulations show that the mean contractility $\rho_{\text{mean}} = \frac{1}{3}(\rho_{11} + \rho_{22} + \rho_{33})$ in the rectangular cell is higher than the square cell where ρ_{11}, ρ_{22}, and ρ_{33} are the normal components of the the contractility tensor ρ_{ij}. The model prediction is in agreement with experimental observations in reference [8] where fibroblasts with higher substrate aspect ratios have higher levels of phosphorylated myosin light chain (p-MLC).

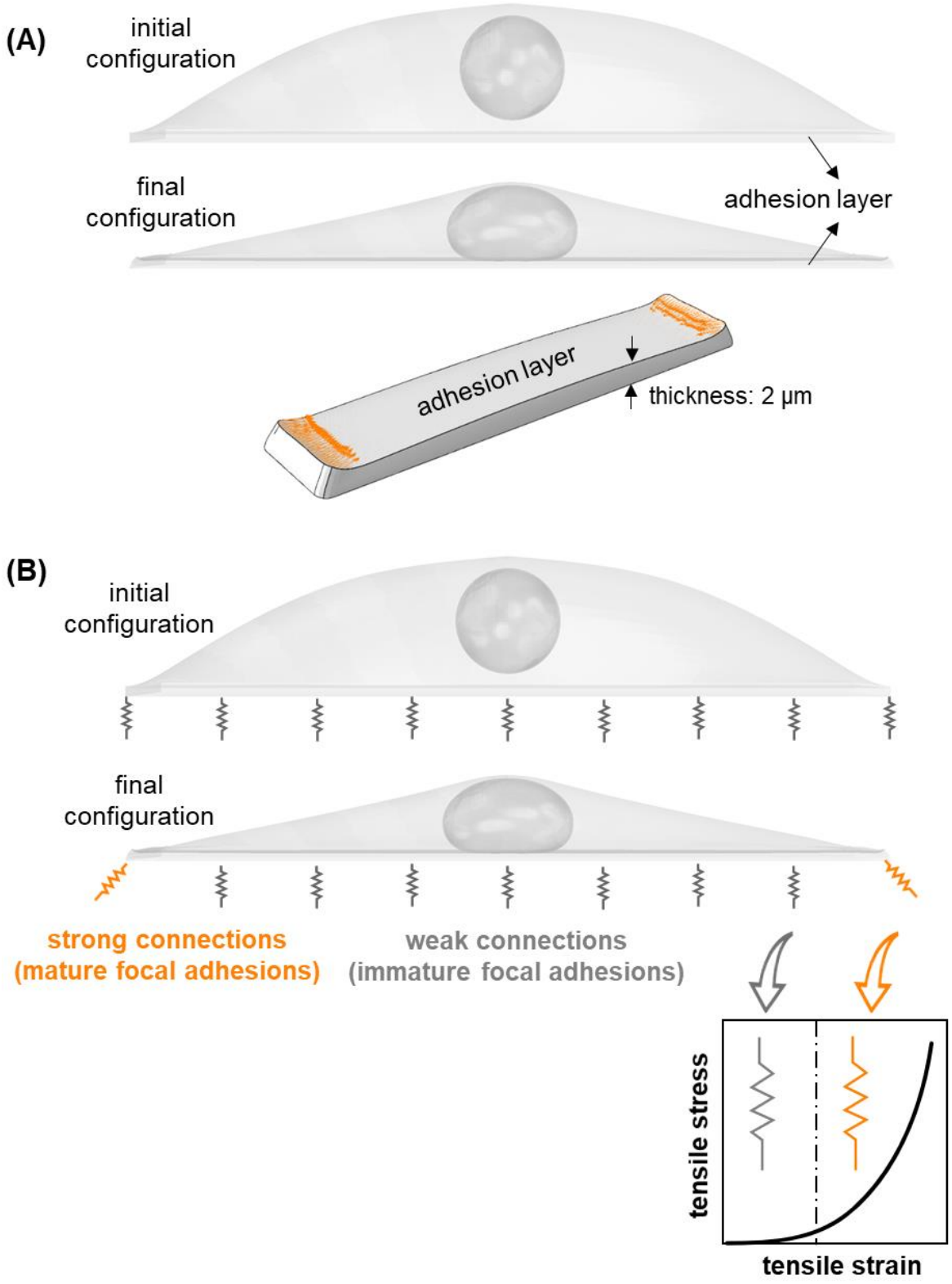

Fig. S4. Tension-dependent formation of mature focal adhesions. (A) A thin layer of elastic material is used in our coarse-grained model to capture the tension-dependent formation of

mature focal adhesions. The adhesion layer is initially soft while it stiffens under tension beyond a critical value of tensile stress. The cell contractility is initially uniform (independent of spatial location) and isotropic (independent of direction) as the cell is seeded on the adhesive substrate (initial configuration). However, for an elongated substrate geometry, the initially uniform and isotropic contractility generates a non-uniform and anisotropic stress field on the adhesion layer. As a result, the adhesion layer experiences higher tensile stresses and stiffens at the two ends. (B) The adhesion layer in our corase-grained model can be regarded as a set of initially soft and uniform nonlinear mechanical elements (representing the initially weak connections between the cell and its rigid substrate) which stiffens under tension beyond a critical value of tensile stress and connects the cell to the substrate (representing the tension-dependent formation of mature focal adhesions).

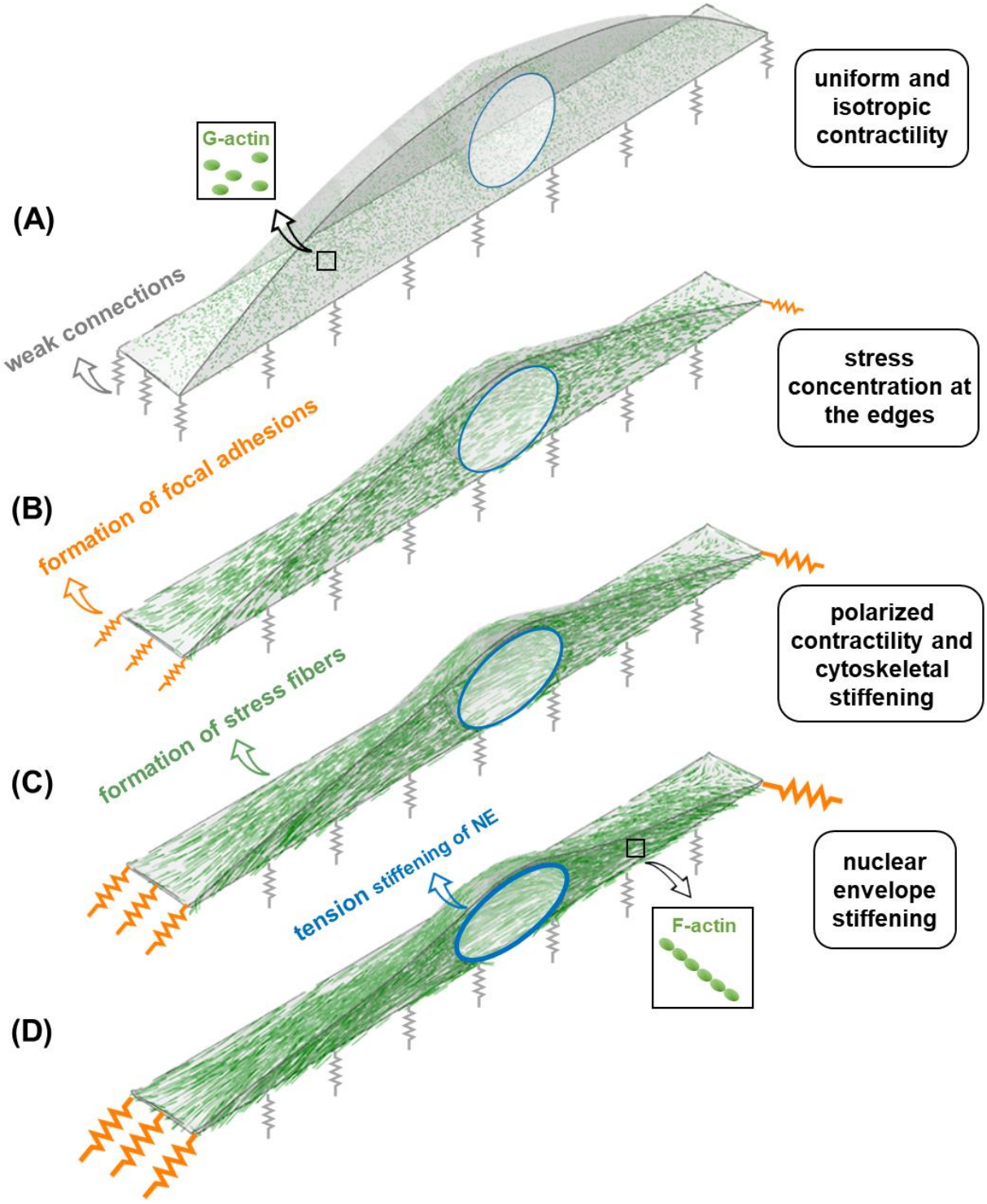

Fig. S5. Transmission of mechanical signals from the substrate to the nucleus in the coarse-grained model. (A) The cell contractility is initially uniform (independent of spatial location)

and isotropic (independent of direction) as the cell is seeded on the adhesive substrate. (B) The uniform and isotropic contractility generates a non-uniform and anisotropic stress field at the cell boundaries where the adhesion layer experiences higher tension at the two ends along the long axis of the cell. Subsequently, the adhesion layer stiffens at the two ends representing the experimentally observed formation of mature focal adhesions which connects the cell to the substrate [2,13]. (C) As the focal adhesions are formed at the two ends, cell contractility is resisted along the long axis of the cell which subsequently generates tension in the cytoskeleton along the long axis of the cell. As a result, the actin filament network stiffens with cytoskeletal tension along the long axis of the cell representing the experimentally observed formation of stress fibers [2,13]. (D) These stress fibers form an arch bridge above the nucleus and impose compressive forces on the nucleus [13,14]. As the nucleus becomes flattened and elongated under the these compressive forces, tension is generated in the nuclear envelope which leads to stiffening of the nuclear envelope representing the experimentally observed (i) tension stiffening of the lamina network [10], and (ii) increase of lamin A/C level with actomyosin contractility [15].

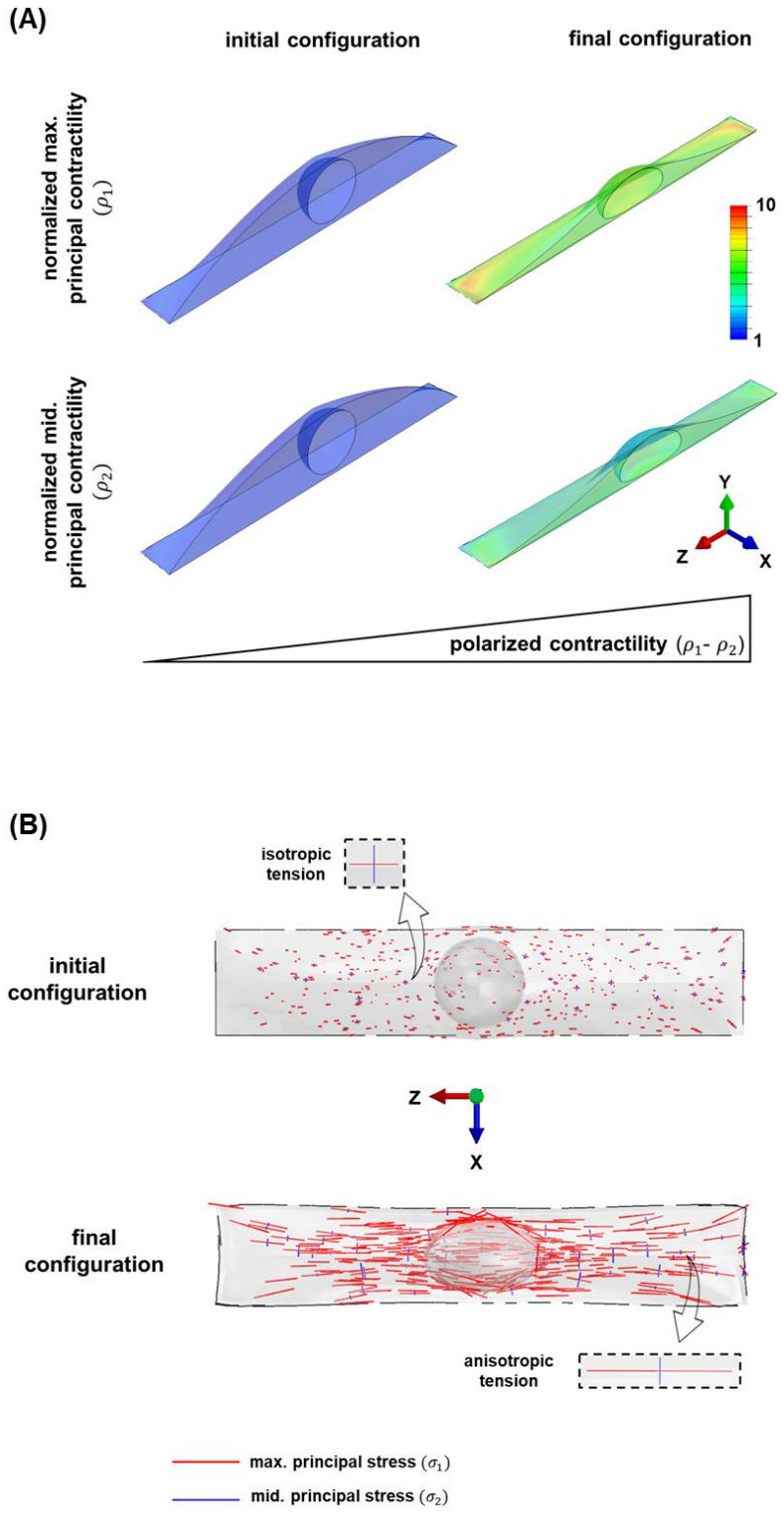

Fig. S6. Elongated substrate geometries induce polarized contractility and polarization of stress in the actin filament network. (A) The cell contractility ρ_{ij} is initially uniform

(independent of spatial location) and isotropic (independent of direction) as the cell is seeded on the adhesive substrate (initial configuration). As a result, the principal contractility components ρ_1 and ρ_2 (primarily along the long (z-direction) and short (x-direction) axes of the cell, respectively) are equal in the initial configuration where ρ_1, ρ_2, and ρ_3 are the eigenvalues of the contractility tensor ρ_{ij}. (B) In addition to the cell contractility ρ_{ij}, the stress in the actin network σ_{ij} are also initially uniform and isotropic as the cell is seeded on the adhesive substrate (initial configuration). As a result, the principal stress components σ_1 and σ_2 (primarily along the long (z-direction) and short (x-direction) axes of the cell, respectively) are equal in the initial configuration where σ_1, σ_2, and σ_3 are the eigenvalues of the stress tensor σ_{ij}. The isotropic contractility, however, generates an anisotropic stress field at the boundaries of an elongated substrate geometry which leads to the formation of mature focal adhesion at the two ends along the long axis of the cell. As a result, cell contractility is more resisted along the long axis of the cell which leads to polarization of the stress in the actin network and polarized contractility along the long axis of the cell.

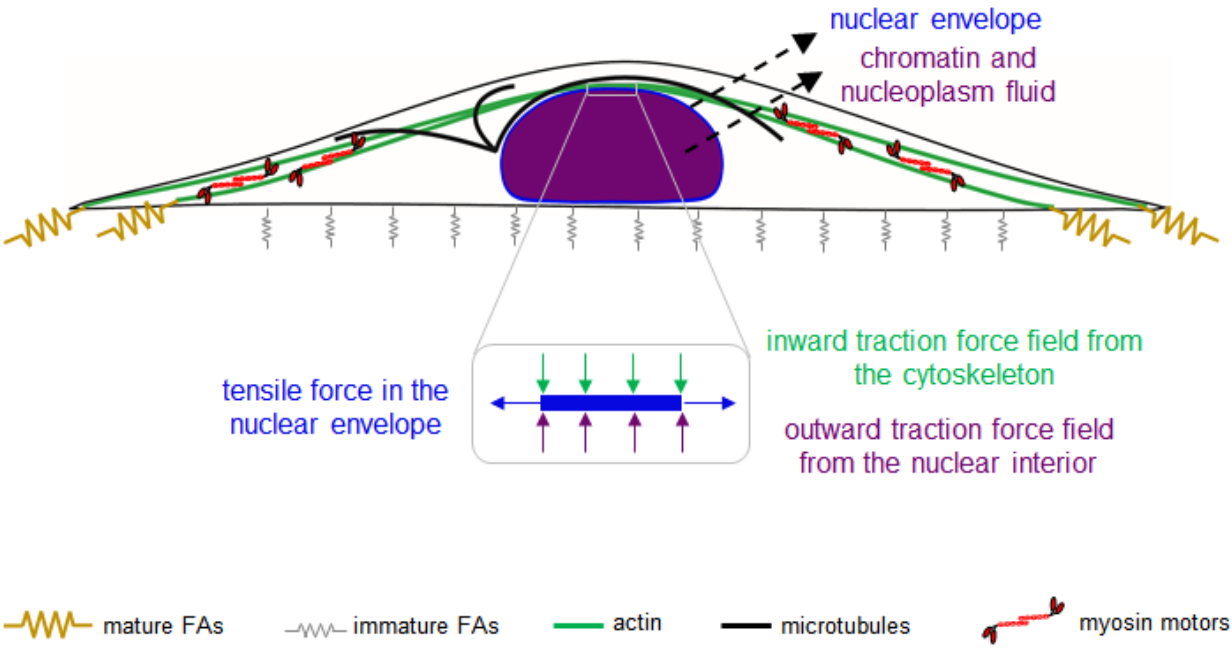

Fig. S7. Mechanical force balance in the nuclear envelope. As cytoskeletal stress fibers impose inward traction forces to the nuclear envelope and compress the nucleus, the nuclear envelope also experiences outward traction forces from the nuclear interior including (i) the mechanical forces due to the resistance of chromatin against deformation, and (ii) the internal pressure due to fluid content. The inward and outward traction forces are balanced by the mechanical forces generated in the nuclear envelope due to the resistance of the nuclear lamina network against deformation.

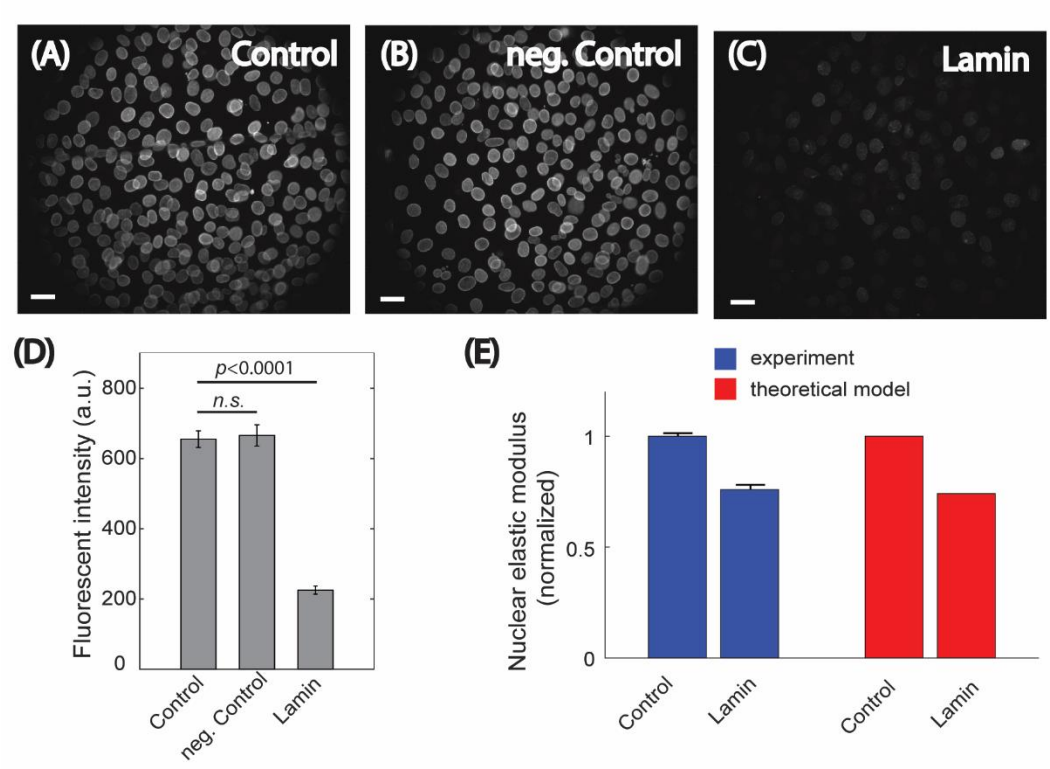

Fig. S8. Experiment and simulation of Lamin A/C knockdown. (A) - (C) Immunofluorescent shows Lamin A/C was successfully knocked down. Scale bar is 20 μm. (D) Quantification shows the knockdown level is about 66%. (E) Our simulations show that a 60% decrease in the initial elastic modulus of the nuclear envelope lamina network (e.g., a 60% decrease of $\widehat{K}^{(\mathrm{I})}$ in equation (S3.7)) yields a decrease of 26% in the effective elastic modulus of the nucleus, which is very similar as calculated in our experiments (24% decrease). The effective elastic modulus of the nucleus in the vertical direction in our theoretical model is calculated as the ratio of the average vertical compressive stress (exerted to the nucleus by the cytoskeleton) to the resulting average vertical compressive strain of the nucleus. The error bar represents the standard error of the mean.

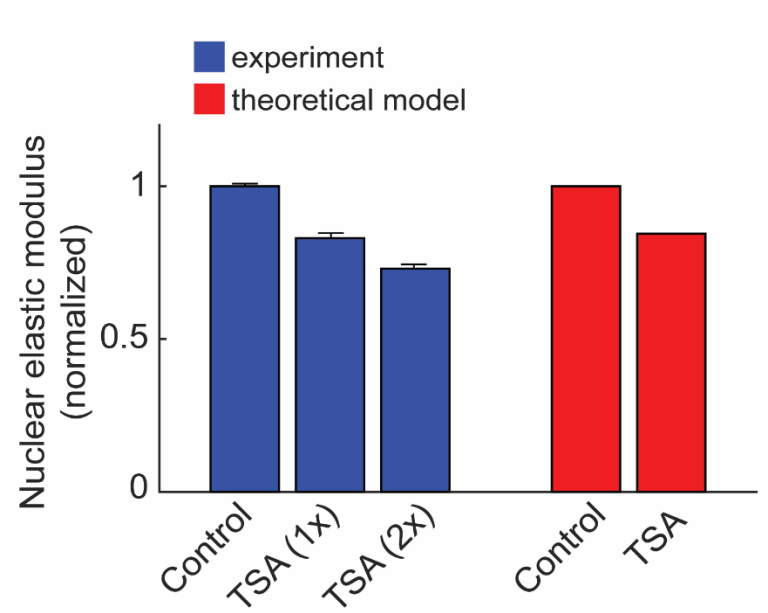

Fig. S9. Experiment and simulation of the nuclear modulus changes upon chromatin decondensation with TSA. The effective elastic modulus of the nucleus in the vertical direction in our theoretical model is calculated as the ratio of the average vertical compressive stress (exerted to the nucleus by the cytoskeleton) to the resulting average vertical compressive strain of the nucleus. A 60% decrease in the elastic modulus of chromatin $\bar{E}$(see equation (S2.2)), captures the nuclear softening observed in our experiments upon TSA treatment. The error bar represents the standard error of the mean. The calculated modulus drops after TSA treatments in experiment are 17% and 27%, respectively. The drop predicted by the simulation is 15.5%.

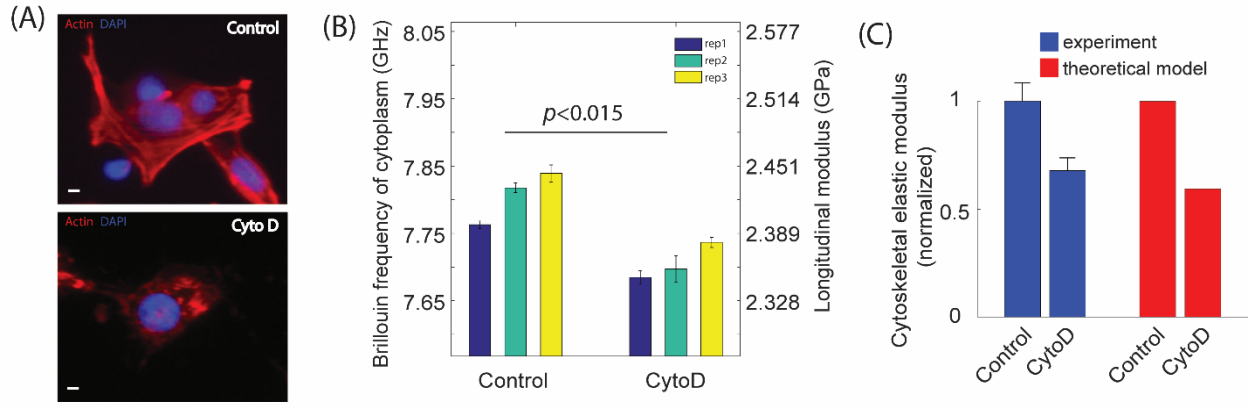

Fig. S10. Experiment and simulation of cytoskeletal modification with CytoD. (A) Confocal fluorescent images show disruption of the actin filament network after treating fibroblasts with CytoD. Scale bar is 2 μm. (B) Experiments show cytoplasm softening after CytoD treatment in fibroblasts cultured on a rigid substrate. (C) Simulation shows the cytoskeletal elastic modulus decreases similar amount as observed in experiment upon CytoD treatment. The decrease of the modulus estimated by experiment is 32%, which agrees with the decrease of 41% observed in the simulation. To simulate the disruption of actin filaments upon cytoD treatment, we decrease the stiffness of the actin network $\mathsf{C}_{ijkl}^{(\mathrm{A})}$ (by setting $\mathsf{C}_{ijkl}^{(\mathrm{F})} = 0$ in equation (S1.8)) and we measure the change in the total modulus of the cytoskeleton in the vertical direction. The error bar represents the standard error of the mean.

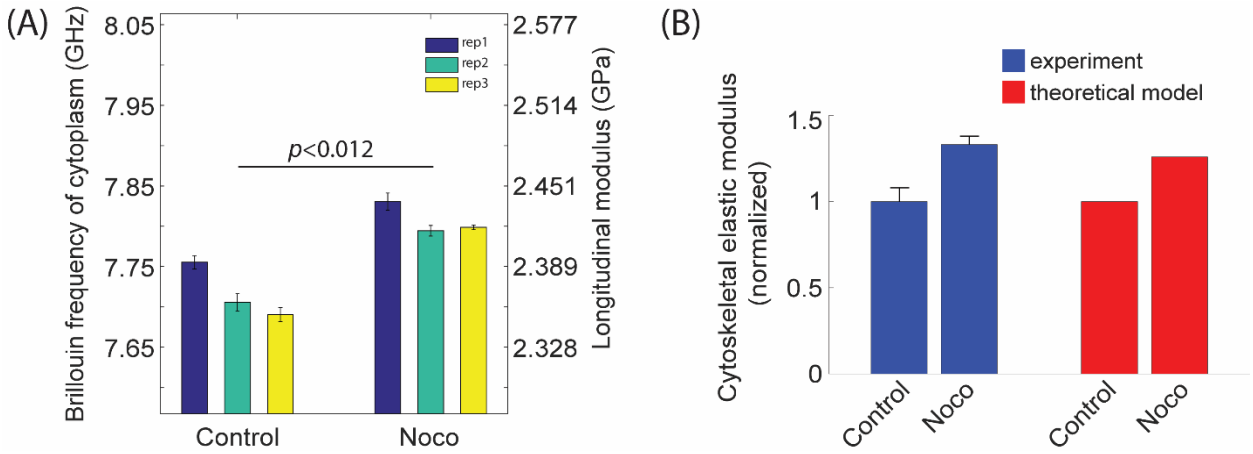

Fig. S11. Experiment and simulation of cytoskeletal modification with Noco treatment. (A) Experiments show cytoplasm stiffening after Nocodazole treatment. (B) Simulation shows the effective elastic modulus of the cytoskeleton increases with disruption of the microtubule network. we simulate the disruption of microtubules by decreasing the stiffness of the microtubule network $\mathsf{C}_{ijkl}^{(\mathrm{MT})}$ (e.g., decreasing $K^{(\mathrm{MT})}$ in equation (S1.4)). The error bar represents the standard error of the mean. The modulus increase estimated by experiment is 33%, which agrees with the increase of 26% observed in the simulation.

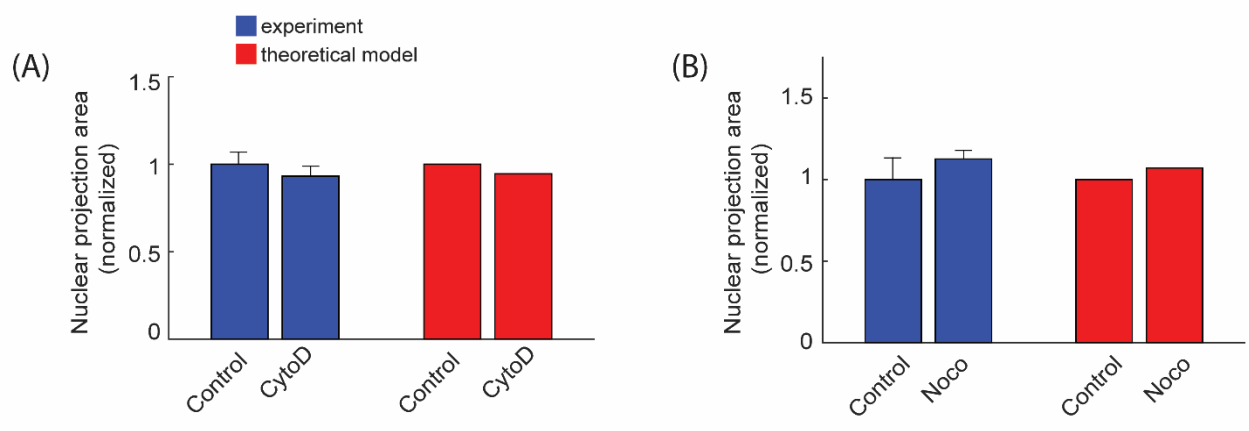

Fig. S12. Experiment and simulation of nuclear projection area changes upon CytoD and Noco treatments. (A) In the simulation, the actomyosin dependent compressive forces on the nucleus decrease with depolymerization of actin filaments which, in turn, decreases the nuclear projected area, which is consistent to the experiment. The decrease of the projection area observed in experiment and simulation is 6.7% and 5.4%, respectively. (B) On the contrary, depolymerization of microtubules upon Nocodazole treatment increases the actomyosin dependent compressive forces on the nucleus. As a result, the simulation predicts the nuclear projected area increases with Nocodazole treatment, similar as we observed in experiment. The error bar represents the standard error of the mean. The increase of the projection area observed in experiment and simulation is 13% and 7%, respectively.

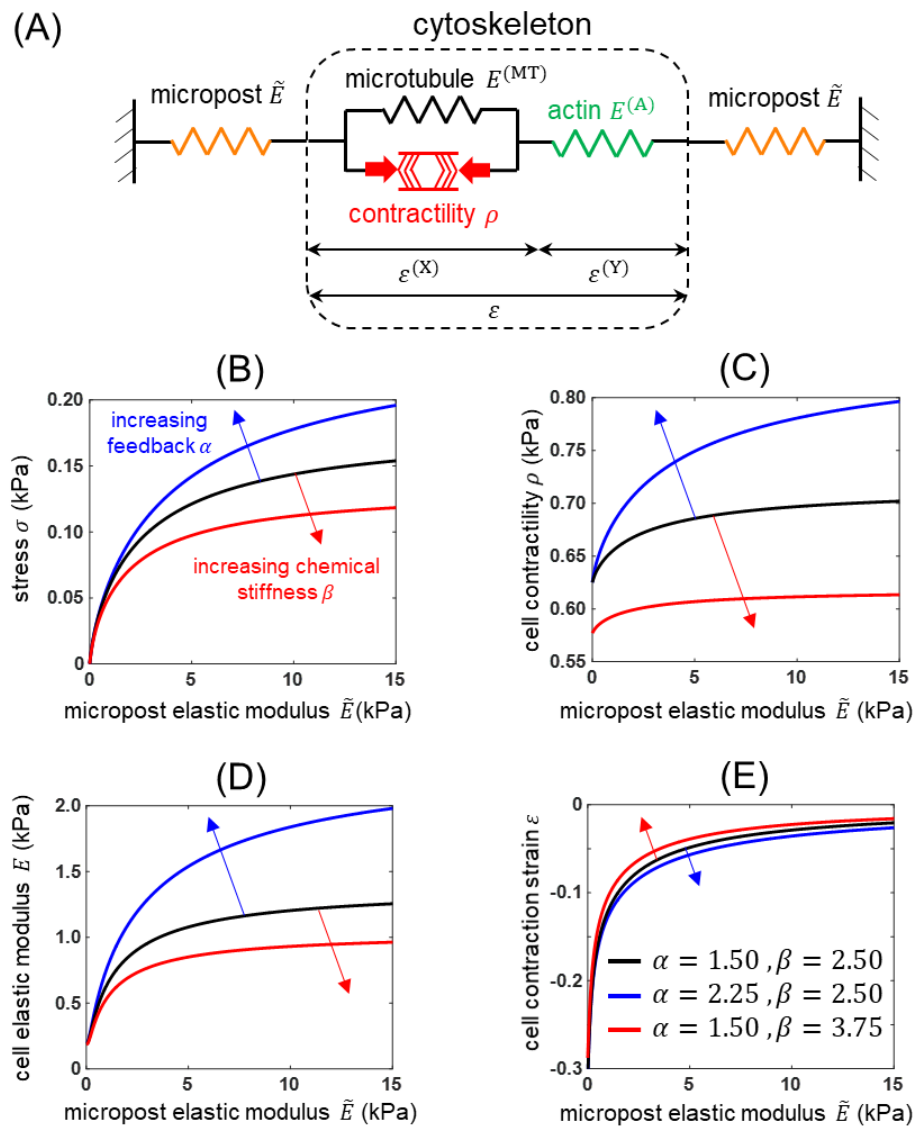

Fig. S13. Cells response to stiffening of their microenvironments by increasing their contractility, stiffness, and force generation. (A) We here present a one-dimensional representation of the three-dimensional cytoskeletal model to show how stiffening of the cell microenvironment impacts the cytoskeleton. (B) As the microposts resist against cell contraction, the tensile stress σ is generated in the actin filament network and the microposts which increases with micropost stiffness $\tilde{E}$. (C) The cell responds to the increase of σ by promoting phosphorylation of myosin motors which increases the cell contractility ρ. (D) Furthermore, as the tension in the actin filament network, σ, increases with $\tilde{E}$, the stiffness of the actin filament network, $E^{(A)}$, and subsequently the cytoskeletal total stiffness, E, increase. Note that $E^{(A)}$ in our

model increases with tension (with the tensile strain $\varepsilon^{(Y)}$) to capture the fact that that cells respond to tension by stiffening of the cytoskeleton through recruitment of actin filaments. (E) The total contractile strain $|\varepsilon| = \left|\varepsilon^{(X)} + \varepsilon^{(Y)}\right|$ decreases with $\tilde{E}$ where $\varepsilon^{(X)}$ and $\varepsilon^{(Y)}$ are the strains of the cytoskeletal components that are in compression ($\varepsilon^{(X)} < 0$) and tension ($\varepsilon^{(Y)} > 0$), respectively.

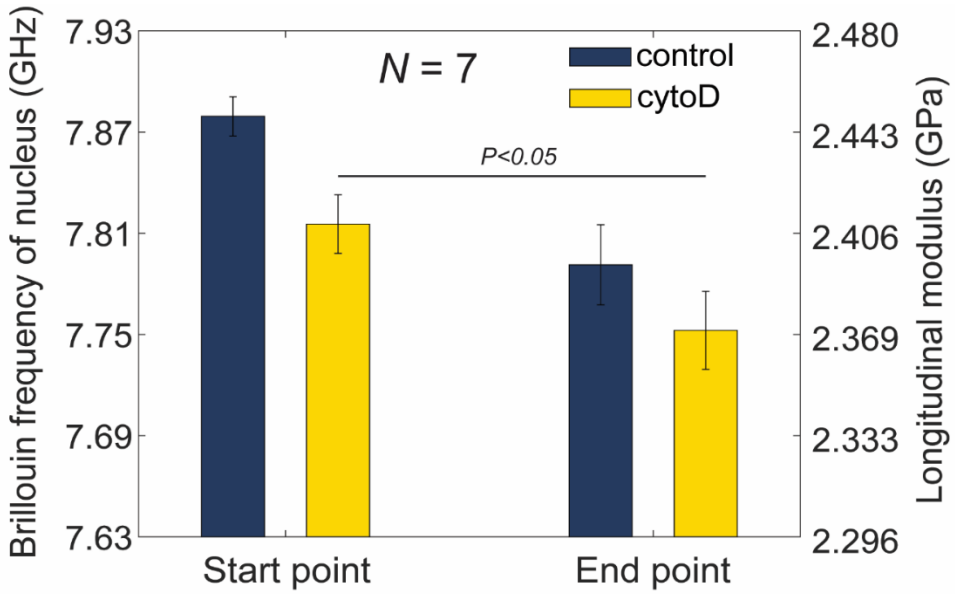

Fig. S14. Statistic results of all cells in detachment experiment. Start point indicates the time point right before trypsinization (t=0); End point indicates the time of 18-20 minutes afterwards**.** The bar plots are the mean value of all cells and the error bar is standard error of the mean (N=7). Our Brillouin microscopy experiments show the mechanical connection between cytoskeleton and nucleus is still functioning after trypsinization.

References

1. Shenoy, V. B., Wang, H. & Wang, X. A chemo-mechanical free-energy-based approach to model durotaxis and extracellular stiffness-dependent contraction and polarization of cells. *Interface Focus* **6**, 20150067 (2016).
2. Alisafaei, F., Jokhun, D. S., Shivashankar, G. V. & Shenoy, V. B. Regulation of nuclear architecture, mechanics, and nucleocytoplasmic shuttling of epigenetic factors by cell geometric constraints. *Proc. Natl. Acad. Sci.* **116**, 13200–13209 (2019).
3. Brangwynne, C. P. *et al.* Microtubules can bear enhanced compressive loads in living cells because of lateral reinforcement. *J. Cell Biol.* **173**, 733–741 (2006).
4. Icard-Arcizet, D., Cardoso, O., Richert, A. & Hénon, S. Cell stiffening in response to external stress is correlated to actin recruitment. *Biophys. J.* **94**, 2906–2913 (2008).
5. Hall, M. S. *et al.* Fibrous nonlinear elasticity enables positive mechanical feedback between cells and ECMs. *Proc. Natl. Acad. Sci.* **113**, 14043–14048 (2016).
6. de Souza Neto, E. A., Peri, D. & Owen, D. R. J. *Computational Methods for Plasticity*. (John Wiley & Sons, Ltd, 2008). doi:10.1002/9780470694626
7. Alisafaei, F., Jokhun, D. S., Shivashankar, G. V. & Shenoy, V. B. Regulation of nuclear architecture, mechanics and nucleo-cytoplasmic shuttling of epigenetic factors by cell geometric constraints. *Proc. Natl. Acad. Sci. U. S. A.* (In Press).
8. Jain, N., Iyer, K. V., Kumar, A. & Shivashankar, G. V. Cell geometric constraints induce modular gene-expression patterns via redistribution of HDAC3 regulated by actomyosin contractility. *Proc. Natl. Acad. Sci.* **110**, 11349–11354 (2013).
9. Buxboim, A. *et al.* Coordinated increase of nuclear tension and lamin-A with matrix stiffness outcompetes lamin-B receptor that favors soft tissue phenotypes. *Mol. Biol. Cell* **28**, 3333–3348 (2017).
10. Stephens, A. D., Banigan, E. J., Adam, S. A., Goldman, R. D. & Marko, J. F. Chromatin and lamin A determine two different mechanical response regimes of the cell nucleus. *Mol. Biol. Cell* **28**, 1984–1996 (2017).
11. Turgay, Y. *et al.* The molecular architecture of lamins in somatic cells. *Nature* **543**, 261–264 (2017).
12. Oakes, P. W., Banerjee, S., Marchetti, M. C. & Gardel, M. L. Geometry Regulates Traction Stresses in Adherent Cells. *Biophys. J.* **107**, 825–833 (2014).

13. Li, Q., Kumar, A., Makhija, E. & Shivashankar, G. V. The regulation of dynamic mechanical coupling between actin cytoskeleton and nucleus by matrix geometry. *Biomaterials* **35**, 961–969 (2014).
14. Khatau, S. B. *et al.* A perinuclear actin cap regulates nuclear shape. *Proc. Natl. Acad. Sci.* **106**, 19017–19022 (2009).
15. Buxboim, A. *et al.* Matrix Elasticity Regulates Lamin-A,C Phosphorylation and Turnover with Feedback to Actomyosin. *Curr. Biol.* **24**, 1909–1917 (2014).